HIGH-FAT DIET ENHANCES TRIGLYCERIDE RECYCLING, IMPAIRS UCP1-MEDIATED THERMOGENIC ACTIVITY, AND CAUSES INSULIN RESISTANCE IN RAT BROWN ADIPOCYTES

DANIEL PEREIRA DA EIRA

A THESIS SUBMITTED TO THE FACULTY OF GRADUATE STUDIES IN PARTIAL FULFILMENT OF THE REQUIREMENTS FOR THE DEGREE OF

MASTER OF SCIENCE

GRADUATE PROGRAM IN KINESIOLOGY AND HEALTH SCIENCE

YORK UNIVERSITY

TORONTO, ONTARIO

JUNE 2019

Abstract

Brown adipose tissue (BAT) is rich in uncoupling protein 1 (UCP1) and dissipates energy through thermogenesis. However, even though BAT mass and its UCP1 content increase under conditions of diet-induced obesity (DIO), marked expansion of the WAT is not prevented, suggesting impairment of BAT-mediated diet-induced thermogenesis (DIT) in obesity. Thus, the objective of this study was to investigate the metabolic and molecular mechanisms that regulated BAT thermogenesis in DIO. To accomplish this, rats were fed a high-fat diet (HFD) for eight weeks. Subsequently, glucose and fat metabolism and the molecular mechanisms underlying these processes were assessed in BAT adipocytes. Despite increasing BAT mass (1.3-fold), UCP1 content (2.1-fold), and isoproterenol (Iso)-induced lipolysis (1.6-fold), HFD reduced UCP1-mediated glucose (62%) and fatty acid (57%) oxidation, and abrogated insulin-stimulated glucose uptake in BAT adipocytes. Furthermore, phosphoenolpyruvate carboxykinase (PEPCK) and glycerol kinase (GyK) contents, as well as glycerol and palmitate incorporation into lipids were all significantly increased (1.8-fold, 2.1-fold, 2-fold, and 1.7-fold, respectively) in HFD BAT. This coincided with 3.6- and 3.7-fold elevations in lipoprotein lipase (LPL) and cluster of differentiation 36 (CD36), respectively, in HFD BAT adipocytes. Morphological analysis also revealed that these adipocytes were more unilocular in appearance. Altogether, these findings provide novel evidence that HFD suppresses UCP1-mediated thermogenesis, shifts metabolism toward triglyceride recycling, and induces insulin resistance in BAT adipocytes. These adaptive responses to chronic HFD are consistent with a mechanism that attenuates the contribution of BAT to DIT and favors the growth of adipose tissue and the development of obesity. Thus reversal of these adaptive metabolic responses of brown adipocytes to DIO could be of therapeutic value for obesity and its related metabolic disorders.

Acknowledgements

Dr. Rolando Ceddia: Two years ago, I could never have imagined accomplishing as much as I did and being as productive as I was. Your love for science resonates within us and inspires us. Although you taught us several lab techniques, I will never forget the life-applicable things I learned from you: to do something to the fullest, no matter how insignificant it may seem, to think about something beyond its face value and that no problem is insurmountable when you trouble-shoot it. Thank you for your guidance and mentorship.

Lab members: To my lab members, thank you for making this one of the more fulfilling experiences of my post-secondary education. We accomplished great things together. Ish, you were always there to help. Thank you for bringing your humor into early morning dissections. Glen, I first learned the Bradford from you. Thank you for teaching me the value of being thorough in my practice of science. Shailee, we worked together from 9-5, Monday to Friday. Although we were both new to the lab, we were able to learn from each other. Thank you for teaching me that mistakes are a crucial part of development and mastery.

Family: To my family, who have supported me every day to pursue anything that I thought I could achieve, I appreciate everything you have done for me. Mom and dad, you came from a small rural town with nothing, yet, you have given us everything. Thank you.

Claudia: Claudia, you encouraged me to pursue this path, leading me to learn new things about myself and evolve as a person. Your support pushed me through some of the more trying times and inspired me to overcome what I thought was insurmountable. Without you, this would have been much harder than what it felt like.

God: De aqui para frente, seja o que Deus quizer.

Table of Contents

List of Abbreviations

aBAT	Aortic brown adipose tissue
AC	Adenylyl cyclase
ACC	Acetyl-CoA Carboxylase
ADP	Adenosine diphosphate
$AdPLA_2$	adipose-specific phospholipase A_2
AMPK	AMP-activated protein kinase
AS160	Akt substrate of 160 kDa
ATGL	Adipose triglyceride lipase
ATP	Adenosine triphosphate
βAdR	β-adrenergic receptor
CACT	Carnitine/acylcarnitine translocase
cAMP	cyclic AMP
CGI-58	Comparative gene identification-58
CNS	Central nervous system
CoA	Coenzyme A
CPT-1/2	Carnitine palmitoyltransferase isoforms 1/2
DAG	Diacylglycerol
DIO	Diet-induced obesity
DIT	Diet-induced thermogenesis
DMN	Dorsomedial nucleus
Epid	Epididymal
ETC	Electron transport chain
F-1,6-diP	Fructose-1,6-diphosphate
F6P	Fructose-6-phosphate
F-FDG	F-labelled fluorodeoxyglucose

FA	Fatty acid (used interchangeably with free FA (FFA) and non-esterified FA (NEFA)
$FADH_2$	Flavin adenine dinucleotide
FATP1	Fatty acid transporter isoform 1
G3P	Glycerol-3-phosphate
G6P	Glucose-6-phosphate
GAPDH	Glyceraldehyde-3-phosphate dehydrogenase
GLUT1/4	Glucose transporter isoform 1/4
GyK	Glycerol kinase
HF	High-fat
HFD	High-fat diet
HSL	Hormone sensitive lipase
iBAT	Interscapular brown adipose tissue
IR	Insulin Resistance
LCFA	Long-chain fatty acid
LDH	Lactate dehydrogenase
Lpl	Lipoprotein lipase
MAG	Monoacylglycerol
mTORC1	Mammalian target of rapamycin complex 1
NADH	Nicotinaminde adenine dinucleotide
NEAT	Non-exercise activity thermogenesis
NEFA	Non-esterified fatty acid (used interchangeably with FA and FFA)
PEPCK-C	Phosphoenolypyruvate carboxykinase (cytosolic isoform)
PET/CT	Positron emission tomography/computed tomography
PFK-1	Phosphofructokinase-1
PGC1α	Peroxisome proliferator-activated receptor gamma coactivator-1 alpha
PGE_2	Prostaglandin E_2
PDK1	Phosphoinositide-dependent kinase 1
PIP3	Phosphatidylinositol 3,4,5-triphosphate

PI3K	Phosphoinositide 3-kinase
PKA	Protein kinase A
PL	Perilipin
PPAR	Peroxisome proliferator-activated receptor
Sc Ing	Subcutaneous inguinal
TAG	Triacylglycerol (used interchangeably with TG)
TCA	Tricarboxylic acid (Cycle)
UCP1	Uncoupling protein-1
VEGF	Vascular endothelial growth factor
VMN	Ventromedial nucleus
WAT	White adipose tissue

List of Figures

1. Introduction

Obesity is a global epidemic that is impacting adults and children alike[1–3]. Of growing concern are the several comorbidities that are associated with obesity, including Type II diabetes, cardiovascular disease, and certain types of cancer[1,2]. Besides being a major concern to public health, it is also a tremendous economic burden for the health care system[1]. The development of obesity is attributed to alterations in energy balance[4], namely reduced energy expenditure and/or increased energy intake[1]. However, the macronutrient composition of a diet also plays a role in determining adiposity[4]. For example, a carbohydrate-rich diet increases glucose availability and triggers the release of insulin, which in turn suppresses lipolysis and enhances the storage of glucose in the liver and skeletal muscles, as well as of triglycerides (TG) in the adipose tissue[4,5]. The ensuing increase in adiposity, particularly in subcutaneous and visceral regions of the body, is what characterizes obesity[6,7].

Pharmacological strategies to reduce energy intake and combat obesity have been used, unfortunately this therapeutic approach has produced disappointing results with respect to weight loss and maintenance of a reduced body weight in the long term[8]. Furthermore, drugs that act on the central nervous system (CNS) to control appetite have numerous deleterious side effects, and end up being withdrawn from the market[8,9]. For instance, the serotonin agonists fenfluramine and dexfenfluramine were used to suppress appetite and facilitate long-term weight loss[10]. Due to non-specific binding to serotonin receptor subtypes, these drugs also caused pulmonary hypertension and valvular heart disease[10,11]. Recently, lorcaserin, a more specifically acting serotonin-receptor agonist, was developed to avoid these adverse side-effects[10]. However, patients still report experiencing headaches, nausea, fatigue and constipation[10]. To avoid the deleterious side effects, scientists have focused on the development of pharmacological strategies that enhance energy

expenditure without targeting the CNS. In this context, the molecular mechanisms that regulate energy storage and dissipation in fat cells has received great attention recently[8]. The intent is to alter adipose tissue function to promote energy dissipation and reduce fat storage, which could be very useful to combat obesity and its related metabolic disorders. It is now well established that two types of adipose tissues exist in humans: white and brown. The former is essentially an energy storage compartment, whereas the latter is specialized in heat production. These two fat depots play a major role in energy metabolism in the body and have been extensively characterized with respect to their morphological and physiological features. BAT has sparked interest in the field of obesity and weight management for its energy dissipating properties. However, little is known regarding the effects of a high-fat diet on the molecular mechanisms that govern the metabolic capacity of BAT. In this context, this thesis aims to determine the implications of DIO for BAT function and metabolism.

2. Literature Review

2.1. WHITE ADIPOSE TISSUE (WAT)

2.1.1. Location and Structure

The white adipose tissue (WAT) is found mainly in subcutaneous and visceral depots and, as previously mentioned, is specialized to store energy in the form of TG[12]. This tissue is primarily composed of adipocytes and stromal cells[13]. The developmental origin of the white adipocyte remains a controversial topic. However, a simplified model of adipocyte lineage suggests that white adipocytes arise mostly from myogenic factor 5 negative ($Myf5^-$) cells[14]. Adipocytes vary in size, depending on the amount of TG that is stored in them[12]. Regardless, the white adipocyte contains a large lipid droplet (LD) that occupies ~90% of the cytoplasm and moves the nucleus and organelles, including mitochondria, to the periphery of the cell[8,12,15]. This confers a unilocular appearance to the cell. WAT mitochondria are sparse in number, more so in larger adipocytes, and display a long, elongated morphology, with randomly oriented cristae[12].

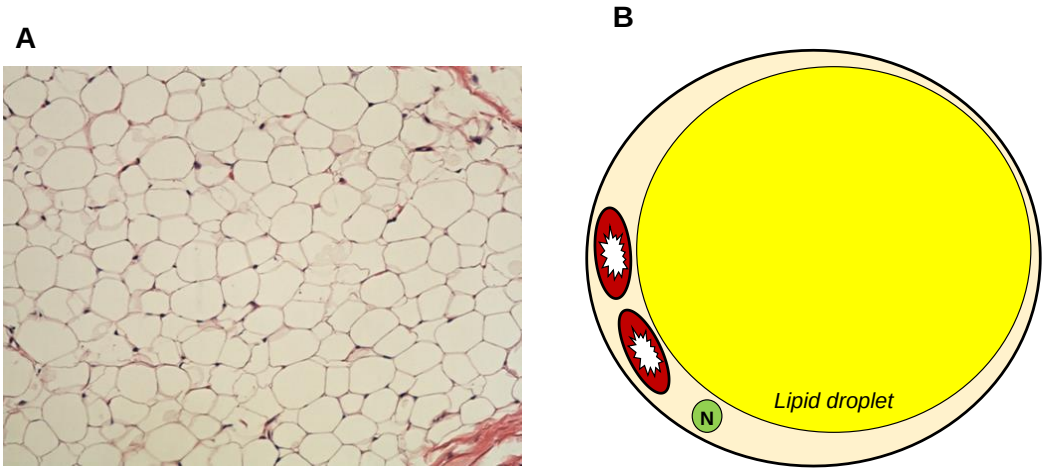

Figure 1: The unilocular white adipocyte. Microscopic image of the subcutaneous inguinal fat with hematoxylin and eosin (H&E) staining at 20x magnification (A)[16]. An illustration depicting the unilocular lipid droplet (LD) in the white adipocyte and its low mitochondrial content (B). N, nucleus.

Accordingly, white adipocytes exhibit limited oxidative capacity, promoting the ideal conditions for the storage of lipids[17]. In situations of increased energy demand, such as exercise or prolonged fasting, these lipids are mobilized by TG hydrolysis, also known as lipolysis, to meet the metabolic needs of peripheral tissues (*e.g.* skeletal muscles, heart, liver)[12,15].

2.1.2. Regulation of Lipolysis

Lipid storage and lipolysis are tightly regulated by insulin and catecholamines in the fed and fasted-state, respectively[13]. Briefly, lipolysis is initiated by the binding of catecholamines to a β-adrenergic receptor[5]. These receptors are coupled to stimulatory G-proteins that activate adenylyl cyclase (AC)[18,19]. AC subsequently increases the formation of cyclic AMP (cAMP), which continues the signaling cascade by activating protein kinase A (PKA)[18]. PKA then phosphorylates perilipin (PL), the protective covering on lipid droplets, causing it to change conformation and release adipose triglyceride lipase (ATGL)-activating comparative gene identification-58 (CGI-58)[5]. Furthermore, the phosphorylation of perilipin causes fragmentation of the lipid droplet, increasing its surface area for contact with lipases[20] and facilitates the interaction of hormone sensitive lipase (HSL) with the lipid droplet[21]. PKA also phosphorylates and activates hormone sensitive lipase (pHSL)[18,22]. Consequently, the complete hydrolysis of TG can occur, with ATGL hydrolyzing TG to diacylglycerol (DAG), phosphorylated HSL (pHSL) hydrolyzing DAG to monoacylglycerol (MAG) and monoacylglycerol lipase hydrolyzing MAG to a free-fatty acid (FFA) and glycerol molecule[5]. The release of FFA into the circulation allows for the transport of this substrate to energy-demanding tissues, which is particularly relevant during periods of exercise or fasting[23].

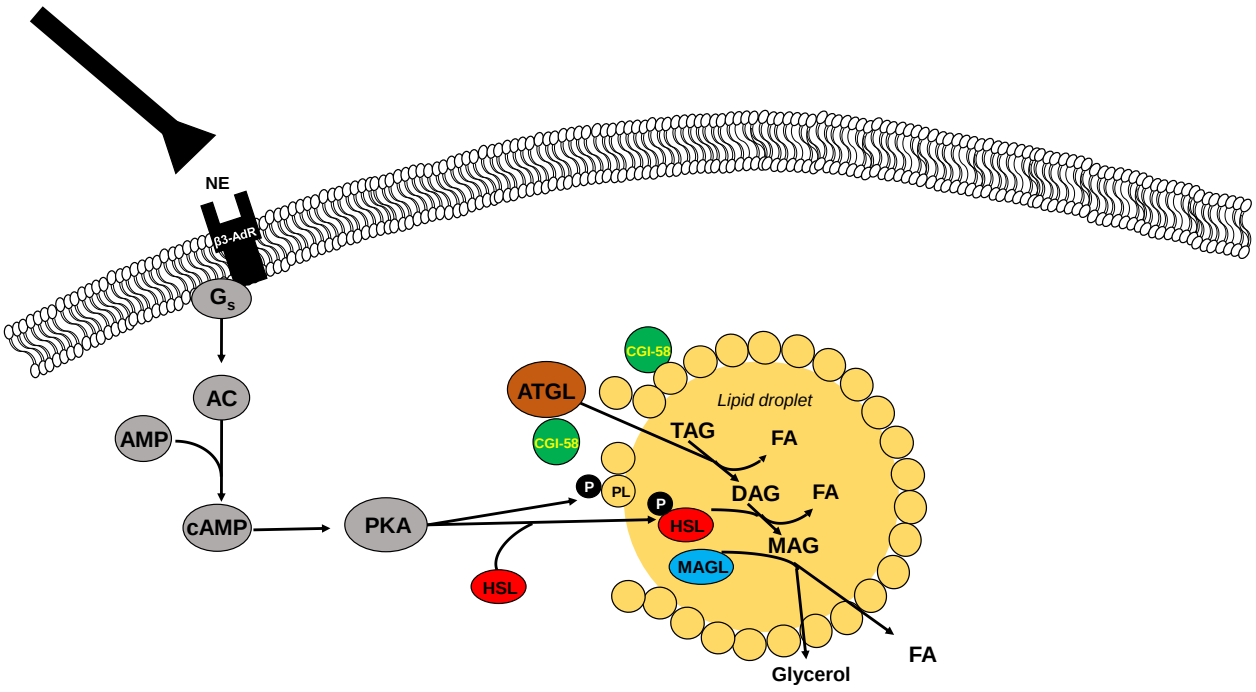

Figure 2: The lipolytic signaling cascade. The release of NE from a sympathetic nerve binds to a β-receptor that is coupled to a stimulatory G-protein. The G-protein subsequently activates AC, which in turn promotes the formation of cAMP. cAMP then activates PKA which phosphorylates PL. PL phosphorylation enables the release of CGI-58, which then binds to and activates ATGL. PKA-mediated phosphorylation also activates HSL. Phosphorylation of PL initiates its dissociation from the lipid droplet, increasing the surface area available for ATGL and pHSL to perform lipolysis. ATGL, pHSL and MAGL hydrolyze TAG, DAG and MAG, respectively, releasing three FAs and a glycerol molecule.

However, a portion of the FAs that are derived from lipolysis are used within the cell to fulfil other purposes[24,25]. For instance, 30-40% of FFAs are re-esterified to TAG, which is dependent on the intracellular production of glycerol-3-phosphate (G3P)[24,25]. A portion of the FFAs released from lipolysis also act as signaling molecules by interacting with a group of transcription factors known as peroxisome proliferator-activated receptors (PPARs)[24,25]. The four PPARs that exist are PPARα, PPARγ-1 and -2 and PPARδ[24]. These transcriptional regulators are activated by the binding of FAs[24]. From there they form heterodimers with other nuclear receptors and interact with transcriptional coactivators, such as peroxisome proliferator-activated gamma coactivor-1α (PGC1α), to promote gene expression[24]. PPARα and PPARδ regulate the

transcription of genes that are involved in oxidative phosphorylation[24]. Conversely, PPARγ is highly expressed in WAT and regulates genes that promote lipid synthesis and storage[24]. In combination with CCAAT/enhancer binding protein (C/EBP), PPARγ has been identified as a crucial regulator for adipocyte differentiation[26]. Thus, lipolysis is an important mechanism that serves both metabolic and transcriptional functions.

In diet-induced obesity (DIO), the dysregulation of lipolytic enzymes can generate lipid intermediates that are harmful to the cell[27]. Under such conditions, the activity of the DAG lipase, HSL, is reduced[27]. Consequently, incomplete lipolysis occurs, leading to the accumulation of the lipid intermediate DAG[27], which has been linked to the development of insulin resistance (IR)[20,28]. Therefore, the regulation of lipolysis is of tremendous importance for the metabolic and transcriptional functioning of the adipocyte.

2.1.3. Insulin-Mediated Lipid Storage

Insulin is a hormone that is crucial for the regulation of glucose and fat metabolism[29]. It is released in response to elevated levels of glucose in the blood and promotes the uptake of glucose and FAs in several tissues[5,6]. Furthermore, insulin is a potent inhibitor of lipolysis, utilizing several mechanisms to interfere with the lipolytic signaling cascade[5]. Firstly, insulin-stimulation activates adipose-specific phospholipase A_2 (AdPLA_2), which increases the production of prostaglandin E_2 ($PGE_{2)}$, that, in turn, interferes with the function of AC and prevents the downstream activation of PKA[5]. Insulin-stimulation also results in the activation of AKT[5]. AKT serves several metabolic functions, however, in the context of lipolysis, it enhances the activation of phosphodiesterase, which suppresses cAMP production and, in turn, inhibits the activity of PKA[5]. AKT also activates mammalian target of rapamycin complex-1 (mTORC1) which suppresses the expression of ATGL

transcripts and reduces the availability of lipolytic enzymes[5]. Finally, insulin promotes the transcription of FSP27, a lipid droplet protein that inhibits lipolysis[5].

In addition to inhibiting TG breakdown, insulin promotes the acute synthesis of TG by increasing the availability of intracellular glucose and FAs[5]. In the context of glucose, insulin enhances the translocation of glucose transporter 4 (GLUT4) to the membrane, providing a channel for glucose entry into the cell[5]. GLUT4 translocation begins with the binding of insulin to its receptor, leading to the phosphorylation of insulin receptor proteins (IRS) by tyrosine kinase[29]. IRS interact with and activate phosphatidylinositol 3-kinase (PI3K)[29], leading to the production of phosphatidylinositol-3,4,5-triphosphate (PIP_3)[29]. PIP_3 subsequently recruits phosphoinositide-dependent kinase 1 (PDK1), mTORC1 and AKT[5,29–31]. Both PDK1 and mTORC1 phosphorylate and activate AKT[29,31]. Once activated, AKT promotes the translocation of GLUT4 to the plasma membrane by phosphorylating and deactivating AKT substrate 160 (AS160), which inhibits the exocytosis of the GLUT4 vesicle[31]. Glucose can thereafter be imported into the cell and be used for the production of G3P, which serves as the backbone for FA esterification and TG synthesis[5]. FA uptake is also increased by insulin-stimulation[5]. Insulin enhances lipoprotein lipase (LPL) activity on the capillary endothelial surface[5,21] which breaks down lipoprotein TG into FAs and glycerol[5]. Circulating TG are derived from dietary fats and are packaged into chylomicrons or very low density lipoproteins (VLDL). The import of FAs is mediated by fatty acid transporter protein 1 (FATP1) and cluster differentiation 36 (CD36) and permits the entry of the hydrolyzed substrates into the adipocyte, where they can be re-esterified into TG[5,21].

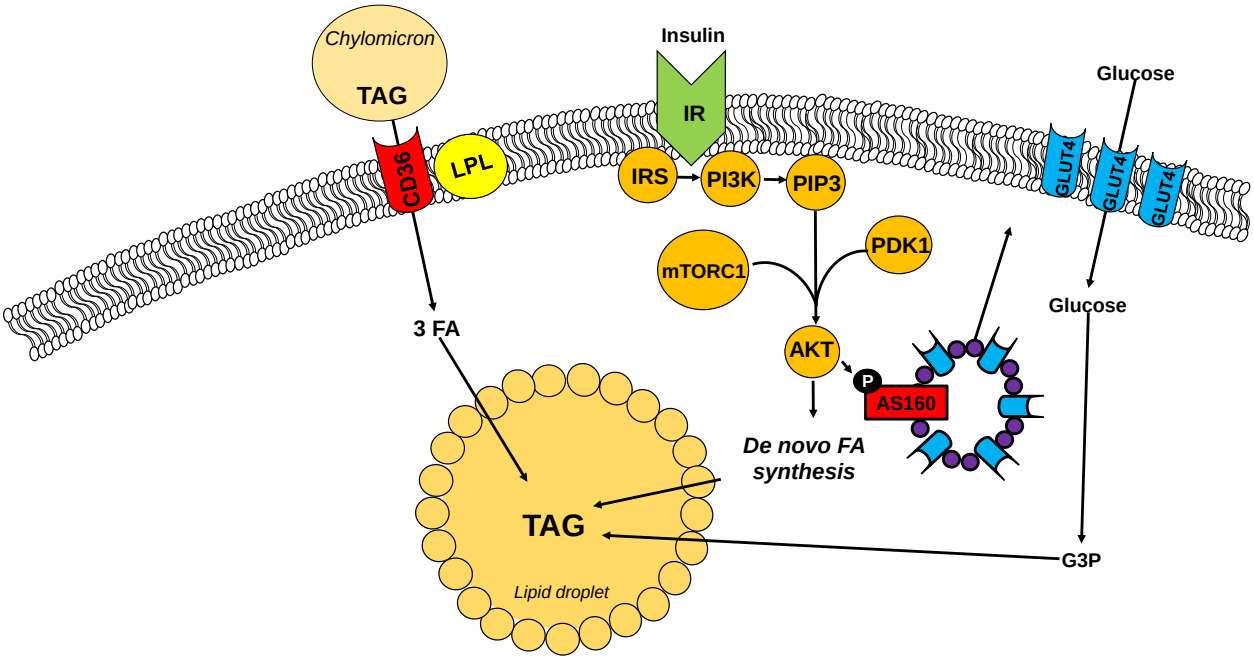

Figure 3: Insulin stimulated glucose and fatty acid uptake in adipocytes. Insulin stimulation activates IRS, which binds to PI3K and enhances the production of PIP_3. In turn, PIP_3 recruits mTORC1 and PDK1 to phosphorylate and activate AKT. AKT then phosphorylates AS160, decreasing its inhibition on the GLUT4 vesicle and allowing it to translocate to the membrane. Membrane-bound GLUT4 increases glucose uptake into the cell, where it can be converted to G3P and used for FA esterification and TG synthesis. AKT also promotes TG formation by enhancing de novo fatty acid synthesis. Furthermore, insulin enhances fatty acid uptake into the cell by facilitating the activity of LPL and fatty acid transporters, including CD36.

In addition to enhancing FA uptake, endogenous FA synthesis is also upregulated by AKT-mediated signaling[5]. Activated AKT phosphorylates and inactivates AMP-activated protein kinase (pAMPK), leaving acetyl-CoA carboxylase (ACC) dephosphorylated and active, allowing it to increase FA synthesis[5]. In concert, these mechanisms provide the adipocyte with the necessary substrates for TG synthesis, promoting the storage of glucose and FAs in the cell[5].

2.1.4. Hyperinsulinemia in DIO

Hyperinsulinemia, or elevated levels of insulin in the circulation, is typical under conditions of chronic obesity and is a compensatory mechanism used to regulate hyperglycaemia[6]. However, as discussed previously, elevated levels of insulin promote the accumulation of lipids

and the development of adiposity[6]. In general, adipose tissue composes 20% and 30% of body mass in men and women, respectively[20]. These percentages can increase dramatically in obese individuals, reaching 50% in the more extreme cases[20]. The expansion of fat mass and the development of obesity precedes the infiltration of immune cells, which have been suggested to contribute to the development of insulin resistance (IR)[5]. A relationship between macrophage content and adipocyte size in multiple fat depots has been reported[32]. Macrophages secrete several factors, known as cytokines, that are implicated in the pathophysiology of IR[33]. Tumor necrosis factor alpha (TNFα) is one such macrophage-derived cytokine[33]. In a murine model with a targeted null mutation of the TNFα gene, obese mice were more responsive to insulin and were better able to regulate blood glucose levels when subjected to a glucose tolerance test[33]. In addition to these systemic effects, tissue-specific adaptations were also observed. In obese $TNF\alpha^{-/-}$ mice, tyrosine phosphorylation of the insulin receptor was increased in both fat and muscle, in comparison to the $TNF\alpha^{+/+}$ obese mice[33]. The authors also identified a reduction in circulating FFA in these animals, which they suggested could be the cause for the improved sensitivity to insulin[33].

In this context, adipose tissue carries tremendous impact for the development of insulin resistance and hyperglycemia. It is important to note that chronically elevated levels of glucose in the blood could potentially lead to the development of full-blown diabetes, where pancreatic β-cell function is impaired[6]. Therefore, understanding the mechanisms that are implicated in lipolysis and lipogenesis under conditions of DIO are crucial for the management of obesity and must be considered for the treatment of related metabolic disorders.

2.1.5. WAT as an Endocrine Organ

WAT also performs endocrine functions by actively releasing adipocyte-derived cytokines, also referred to as adipokines[34]. Leptin, for example, is released in proportion to the quantity of

adipose tissue and signals to the hypothalamus to promote satiety[35,36]. When adipose tissue stores are low, leptin secretion is reduced and neuropeptide Y secretion is increased to promote hunger and food intake[26]. In the context of energy metabolism, leptin plays an important role in increasing sympathetic nervous system (SNS) activity and energy dissipation[35]. This was demonstrated in leptin-deficient mice that exhibited lower body temperatures and suppressed sympathetic nerve activity[37] . Adiponectin is another adipocyte cytokine (adipokine) that is expressed in both WAT and BAT[38]. Unlike leptin, adiponectin release is reduced in obese, insulin resistant individuals either due to genetic factors that affect the expression of the adiponectin gene or lifestyle factors causing obesity, including diet[38]. Adiponectin has been shown to improve insulin sensitivity in insulin resistant models[38] and plays a role in regulating cold-induced thermogenesis in the energy-dissipating BAT[39].

In summary, WAT is a multi-functional tissue that fulfills several metabolic and endocrine functions. However, the accumulation of fat can lead to adverse consequences including the development of insulin resistance and diabetes. It is therefore important to consider DIO and its implications for energy storage in adipose tissue.

2.2. BROWN ADIPOSE TISSUE (BAT)

2.2.1. Origin, Location and Structure

In rodents, BAT can be found in the axillary and interscapular regions[12]. Until recently, BAT was thought to only be relevant in human infants and small mammals for the purpose of thermoregulation[40]. However, recent studies have shown active BAT in human adults, sparking interest in this tissue as a potential therapeutic tool for the treatment of obesity[40,41]. BAT cells, or brown adipocytes, share a common origin with muscle cells, originating from myogenic-regulatory factor 5-expressing cells ($Myf5^{+}$)[42]. The proliferation of BAT preadipocytes is regulated by NE

and its stimulation of the β_1-cAMP pathway[18]. When treated with NE, brown preadipocytes increase their formation of cAMP, leading to the activation of PKA[43]. In turn, PKA activation increases the expression of ribonucleotide reductase[43], an enzyme that performs the limiting step for DNA synthesis and cell proliferation[18]. NE also promotes the differentiation of brown adipocytes through a cAMP/PKA/cAMP response element binding protein (CREB) pathway. In this pathway, NE binds to β3-AdR, increasing the formation of cAMP and, in turn, the activation of PKA[18]. Thereafter, PKA phosphorylates CREB, which promotes the expression of enzymes and other transcription factors, including PGC1α, that contribute to the differentiation of these thermogenic cells[18,42]. Contrary to white adipocytes, brown adipocytes contain several lipid droplets (multilocular appearance) and are relatively smaller in diameter; 15-50 μm[12]. These adipocytes are also abundant in mitochondria that are spherical with laminar cristae[12]. The elevated mitochondrial content in this tissue is what gives it its brown appearance[15]. These mitochondria are also characteristically rich in uncoupling protein 1 (UCP1), which uncouples electron transport from adenosine triphosphate (ATP) production, resulting in the production of heat, also known as thermogenesis[15,42].

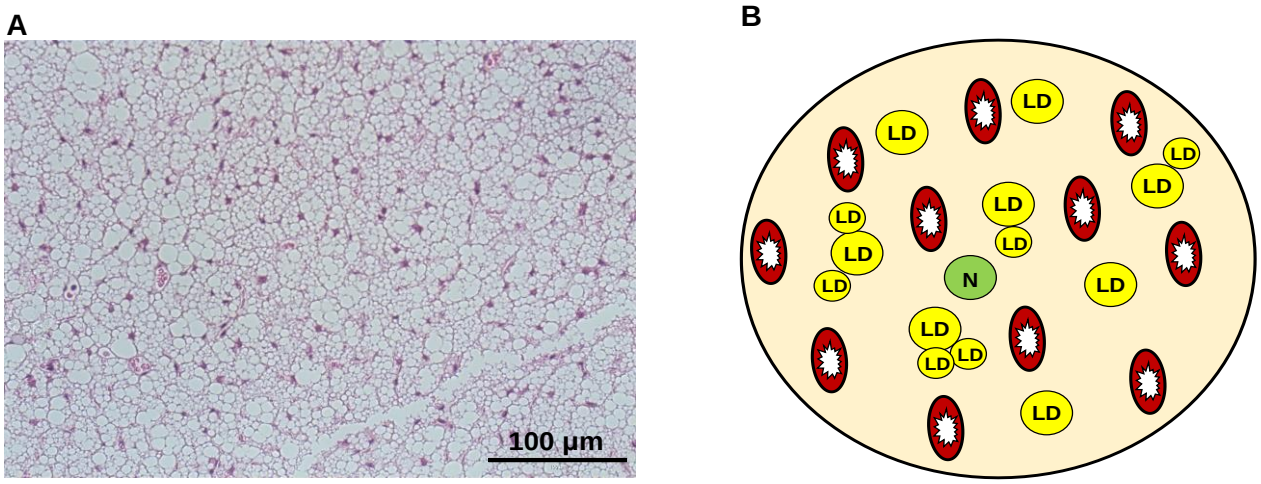

Figure 4: The multilocular brown adipocyte. Microscopic image of iBAT with hematoxylin and eosin (H&E) staining at 40x magnification (A). An illustration depicting the multilocular appearance of the brown adipocyte and its high mitochondrial content (B). N, nucleus.

2.2.2. Glucose and Fatty Acid Metabolism: Glycolysis, β-Oxidation and the TCA Cycle

UCP1-mediated thermogenesis uncouples the oxidation of glucose and FAs from the production of ATP[40,44,45]. In the context of glucose, once it is imported into the cell, it can be diverted to glycolysis[45]. The glycolytic pathway starts with the ATP-consuming phosphorylation of glucose by hexokinase[45]. Although this seems counterintuitive to the objective of energy production, the early consumption of ATP in glycolysis is considered an important investment for the latter stages of ATP synthesis[46]. Phosphoglucose isomerase subsequently converts Glucose-6-phosphate (G6P) into fructose-6-phosphate (F6P), which is, in turn, phosphorylated by phosphofructokinase-1 (PFK-1) to produce fructose-1,6,-diphosphate (F-1,6-diP)[45]. Aldolase then breaks this molecule into two three-carbon compounds, glyceraldehyde-3-phosphate and dihydroxyacetone phosphate (DHAP)[45]. However, DHAP can also be converted to glyceraldehyde-3-phosphate by phosphotriose isomerase, providing the glycolytic pathway with a second energy producing molecule[45,46]. The glyceraldehyde-3-phosphate molecules are subsequently processed by glyceraldehyde-3-phosophate dehydrogenase (GAPDH) for the production of two 1,3-diphosphoglycerate molecules[45]. This step involves the reduction of NAD^+ to NADH and the phosphorylation of glyceraldehyde-3-phosphate with an inorganic phosphate[47]. Phosphoglycerate kinase then catalyzes the conversion of 1,3-diphosphoglycerate to 3-phosphoglycerate, phosphorylating an ADP molecule to produce ATP in the process[45]. 3-phosphoglycerate is then converted to 2-phosphoglycerate and phosphoenolpyruvate (PEP), in sequence, by phosphoglycerate mutase and enolase, respectively[45].

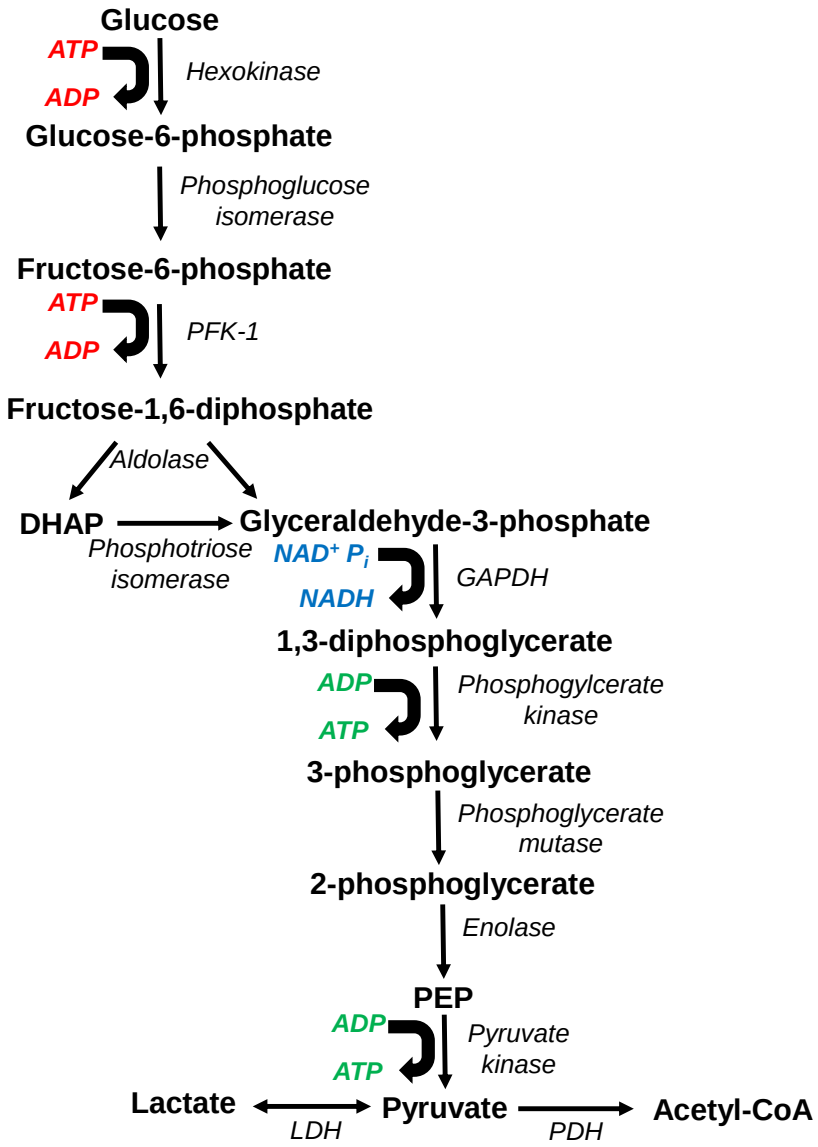

Fig. 5: The glycolytic pathway**.** Glucose is phosphorylated by to form glucose-6-phosphate (G6P), which in turn is converted to fructose-6-phosphate and phosphorylated again by phosphofructokinase-1 (PFK-1). Fructose-1,6-diphosphate is then broken into dihydroxyacetone phosphate (DHAP) and glyceraldehyde-3-phosphate. However DHAP can also be converted to glyceraldehyde-3-phosphate by phosphotriose isomerase. Glyceraldehyde-3-phosophate dehydrogenase (GAPDH) then converts glyceraldehyde-3-phosphate to 1,3-diphosphoglycerate, reducing NAD^+ to NADH in the process. Subsequently, 1,3-diphosphoglycerate is converted to 3-phosphoglycerate by phosphoglycerate kinase, resulting in the first production of an ATP molecule in the glycolytic pathway. From there, 3-phosphoglycerate is processed into 2-phosphoglycerate by phosphoglycerate mutase. Subsequently, enolase catalyzes the conversion of 2-phosphoglycerate to phosphoenolpyruvate (PEP). Finally, PEP is used by pyruvate kinase to phosphorylate a second ADP and produce pyruvate. Pyruvate can then be used for lactate production or it can be converted into Acetyl-CoA. The conversion of pyruvate to lactate is reversible.

Finally, pyruvate kinase phosphorylates a second ADP molecule, converting phosphoenolpyruvate to pyruvate and concluding glycolysis[45]. In total, this process involves the synthesis of four ATP molecules and the breakdown of two, resulting in the net production of two ATP molecules[47]. Pyruvate can thereafter be reversibly converted to lactate by lactate dehydrogenase (LDH)[46,48], or it can be transported into the mitochondria and decarboxylated by pyruvate dehydrogenase (PDH) to form acetyl-CoA[48].

If pyruvate is converted to Acetyl-CoA, it can enter the Tricarboxylic Acid (TCA) Cycle, which is important for the production of metabolic substrates that drive the ETC[49]. The first step of the TCA Cycle is the condensation of Acetyl-CoA with oxaloacetate, which is mediated by the enzyme citrate synthase to produce citrate[50]. Aconitase then converts citrate to isocitrate which serves as a precursor for α-ketoglutarate formation[50]. The decarboxylation of isocitrate to α-ketoglutarate is catalyzed by isocitrate dehydrogenase and produces a molecule of CO_2[50]. More importantly, this step leads to the reduction of NAD^+ to NADH, which is an important reducing equivalent for the production of ATP in the ETC[50,51]. Subsequently, α-ketoglutarate is converted to succinyl-CoA by α-ketoglutarate dehydrogenase, which, in parallel, produces the second CO_2 and NADH molecules in the TCA Cycle[50,51]. Succinyl-CoA is thereafter converted to succinate by succinic thiokinase[50]. This step is also marked by the phosphorylation of GDP to GTP[50]. Succinate dehydrogenase then converts succinate to fumarate[50]. In parallel, FAD is reduced to $FADH_2$, which is also important for the function of the ETC[50]. The following step involves the hydration of a double bond in fumarate that is catalyzed by fumarase, resulting in the production of malate[50]. From here, malate dehydrogenase regenerates an oxaloacetate molecule from malate and produces $NADH_2$[50]. Oxaloacetate can then re-enter the TCA cycle by interacting with another acetyl-CoA and initiating the aforementioned sequence of events[50].

The initial stages of FA metabolism is different from that of glucose; however, both converge at the TCA Cycle. FAs enter the cell and are esterified to Coenzyme A (CoA) to make Acyl-CoA. The transport of the FA into the mitochondria is dependent on a carnitine shuttle, which is composed of carnitine palmitoyltransferase I (CPT1), carnitine/acylcarnitine translocase (CACT) and carnitine palmitoyltransferase II (CPTII)[44]. The first step of mitochondrial fatty acid import involves the CPT1-mediated conversion of Acyl-CoA to acylcarnitine[44]. This step is rate-limiting for the oxidation of FAs in the mitochondria[44]. Following this, CACT facilitates the import of acylcarnitine through the inner mitochondrial membrane and into the matrix[44]. Finally, CPTII re-esterifies acylcarnitine to Acyl-CoA, releasing the carnitine and preparing the FA for oxidation[44]. Once inside the mitochondria, Acyl-CoA undergoes β-oxidation, which is the splitting of the Acyl-CoA into two carbon Acetyl-CoAs[44]. β-oxidation requires the action of four enzymes in sequence[44]. The first stage of β-oxidation is catalyzed by acyl-CoA dehydrogenases, of which there are also four; short-chain acyl-CoA dehydrogenase, medium-chain acyl-CoA dehydrogenase, long-chain acyl-CoA dehydrogenase and very long-chain acyl-CoA dehydrogenase[44,52]. As their names imply, they act on fatty acid chains of varying lengths and convert acyl-CoA to 2-Enoyl-CoA[52]. 2-Enoyl-CoA is converted to 3-hydroxyacyl-CoA by 2-Enoyl-CoA hydratase[52]. 3-hydroxyacyl-CoA dehydrogenase is the third enzyme involved in β-oxidation and its function is to convert 3-hydroxyacyl-CoA to 3-oxoacyl-CoA[52]. The final step of β-oxidation is the cleavage of 3-oxoacyl-CoA to acetyl-CoA and a saturated acyl-CoA[52]. This final step is catalyzed by 3-oxoacyl-CoA thiolase[52]. The residual acyl-CoA undergoes additional rounds of β-oxidation for the continuous generation of Acetyl-CoA[52]. Once formed, Acetyl-CoA enters the TCA Cycle to drive the production of the metabolic equivalents required for oxidative phosphorylation; NADH and $FADH_2$[50,51,53].

2.2.3. Glucose and FA Metabolism: Electron Transport Chain (ETC), Oxidative Phosphorylation and Mitochondrial Uncoupling

The oxidation of glucose and fatty acids in the TCA Cycle generates the reducing agents NADH and $FADH_2$[53], both of which drive oxidative phosphorylation in the ETC[49]. NADH dehydrogenase and succinate dehydrogenase receive electrons from NADH and $FADH_2$, respectively[53]. These electrons are passed onto Coenzyme Q which acts as a mobile transporter for these electrons to the next ETC complex[53]. The electrons are shuttled to complex III, cytochrome c and cytochrome c oxidase, in sequence[53]. Finally, the electrons are used to reduced O_2 to H_2O[54]. As these electrons are transported across the complexes, protons are pumped into the intermembrane space of the mitochondria[54]. Pumping occurs at Complexes I, III, and IV and leads to the formation of a proton gradient between the intermembrane space and the mitochondrial matrix[40,55]. This electrochemical gradient is dissipated as the protons enter the matrix through the ATP synthase complex in a process that leads to the generation of ATP[40,55]. However, if UCP1 is present and active, protons have an alternative entry into the mitochondrial matrix without going through ATP Synthase[56]. The re-entry of protons into the matrix that occurs independently of ATP Synthase, is known as proton leak, or State 4 respiration, and uncouples electron transport from ATP synthesis[57], releasing the substrate-derived chemical energy as heat[40].

2.2.4. Thermogenesis is Regulated by SNS Activity

In BAT, UCP1-mediated thermogenesis is induced by activation of the SNS[18]. BAT is highly innervated and rich in β3-AdR[18]. As previously mentioned, the stimulation of these receptors by NE initiates a lipolytic signaling cascade that activates the hydrolytic enzymes ATGL and HSL[18]. The hydrolysis of TG in brown adipocytes increases intracellular FFAs that serve to activate UCP1[19]. The long chain fatty acid (LCFA)-shuttling model has been proposed to explain

how UCP1 is activated in brown adipocytes. In this model, LCFAs interact through their hydrophobic tails to UCP1 and bind protons, whereby a conformational change in UCP1 ensues, translocating the LCFA and proton to the mitochondrial matrix[58]. The hydrophobic tail of the LCFA does not allow it to dissociate from UCP1[58], thus, after the proton is released into the matrix, the LCFA is returned to the opposite side of the inner mitochondrial membrane, where it can facilitate the translocation of another proton[58].

2.2.5. An Alternative Fate for Glucose and FAs in the BAT

However, as described earlier, not all FAs derived from lipolysis enter the mitochondria for oxidation or mitochondrial uncoupling. Many FFA return to WAT and BAT to be re-esterified into TAG[59]. This means that a constant source of G3P is required in these tissues[60]. Glycerol is derived from the lipolysis of TG, glycolysis or glyceroneogenesis[59,60]. Firstly, following complete lipolysis, or the hydrolysis of the three FAs that are esterified to a glycerol backbone, glycerol is released and can be used for re-esterification[59]. Contrary to WAT, BAT possesses Glycerol Kinase (GyK), allowing it to phosphorylate the free glycerol and use it for TAG re-synthesis[59,60]. The second source of glycerol is glycolysis. In the fed-state, BAT increases its uptake of glucose from the ciruclation[61,62] and favors the storage of TG within its adipocytes[59]. Insulin-stimulation increases glucose uptake and glycolysis, which enhance the production of ATP and 3-phosphoglycerol[59,60]. Both of these products are required for FA esterification; 3-phosphoglycerol is the backbone for TAG synthesis and ATP is required for esterification to take place[59]. In BAT, much of the available glycerol for TG synthesis is made in a process known as glyceroneogenesis, which is driven by phosphoenolpyruvate carboxykinase (PEPCK)[60]. The expression of PEPCK is regulated by several transcription factors, including PPARγ[59]. PEPCK-mediated conversion of oxaloacetate to phosphoenolpyruvate is the defining step for classical glyceroneogenesis[60].

Interestingly, in BAT, PEPCK activity is disproportionately high relative to the amount of glycerol being produced[60]. This can be attributed to the fact that in BAT is used for the dual purpose of fueling *de novo* glycerol production and to replenish Citric Acid Cycle intermediates that are required to maintain high rates of TG breakdown/re-esterification and oxidation[60]. Mottilo et al. investigated glyceroneogenesis and lipid turnover in BAT and WAT and found that lipolysis and TG re-synthesis are linked[17]. In fact, knocking out ATGL eliminated β_3 adrenoreceptor-specific enhancement in glycerol incorporation into TG and mitochondrial respiration, and decreased PEPCK protein content in brown adipocytes[17]. This led the researchers to propose a possible fatty acid cycling mechanism within BAT, as well as a relationship between TG synthesis, lipolysis and oxidation[17].

2.2.6. Cold and Exercise-Mediated Regulation of BAT Function

The SNS-induced activation of UCP1 is of tremendous physiological importance in the context of cold tolerance and thermogenesis[18]. The first response to acute cold-exposure is shivering, where heat is generated by ATP-consuming muscular contractions[56]. Following prolonged cold-exposure, shivering subsides and is replaced by non-shivering thermogenesis[18,56]. The distribution of the produced heat to the periphery is facilitated by the extensive vascularization of BAT[42]. The heat-generating capacity of BAT is suggested to be an evolutionary mechanism to cope with cold-stress in hibernating animals and in humans[18]. The cold-induced activation of BAT has received great attention for its therapeutic potential in the management of obesity. Sepa-Kishi et al. used a rat model of cold-acclimation and showed that although cold-exposed animals ate more, they had significant reductions in Sc Ing and Epid fat masses[16].

The cold-induced activation of BAT also plays a broader role in the context of circulating metabolic substrates[63]. BAT effectively accelerates the clearance of dietary TG and glucose from

the circulation[63] and oxidizes fat to a greater extent[16]. This was demonstrated by Sepa-Kishi et al. in isolated BAT adipocytes, where they measured basal and oligomycin (Oligo)-induced palmitate oxidatiion[16]. Both basal and Oligo-induced palmitate oxidation were enhanced to a similar degree in the BAT of cold-acclimated animals[16]. They also found no significant difference between basal and Oligo-induced oxidation in the brown adipocytes of the cold-exposed animals leading them to conclude that mitochondrial uncoupling accounted for much of the FA oxidation occurring in brown fat[16]. Interestingly, BAT adipocytes enlarge with cold-exposure due to TAG storage[16]. Although this may seem contradictory to the notion of thermogenesis, it is a mechanism used by the adipocytes to provide the thermogenic machinery with readily available substrate[16]. The cold-induced activation of BAT is met with the recruitment of brown-like cells in WAT, known as beige adipocytes, that exhibit similar metabolic and morphological characteristics[23].

2.2.7. Beige Fat: Recruitment and Activation of Remote BAT

Beige fat arises from WAT in a process known as "browning"[23,64]. This conversion occurs in adipocytes that are subject to specific stimuli, including cold and β-adrenergic stimulation[40,65] and is more common in the subcutaneous fat where the adipocytes exhibit greater plasticity to "brown"[23]. Cold-exposure triggers morphological and molecular adaptations in these adipocytes, causing them to become more multilocular and abundant in UCP1, although not to the same extent as brown adipocytes[65]. Interestingly, these adipocytes do not rely on mitochondrial uncoupling to the same extent as BAT for thermogenesis[16]. Instead, thermogenesis is achieved through an energy-consuming phenomenon where TGs undergo a hydrolysis/re-esterification cycle[16].

The browning of WAT is also promoted by exercise[64]. This was observed by Wu et al. in the Sc Ing fat of treadmill exercised rats. It is important to note that the Sc Ing fat depot did not adapt homogenously. Rather the adipocytes located centrally in the tissue possessed a greater

capacity to adapt thermogenic properties[64]. The site-specific differences in this tissue grants it metabolic flexibility whereby the peripheral areas can store TG and the centralized portion of the tissue can dissipate this stored energy[23]. Similar to cold-exposure the thermogenic adipocytes in this fat pad become more multilocular in appearance with endurance training, express higher levels UCP1 and PGC1α protein contents, and oxidized palmitate to a greater extent[64]. Interestingly, exercise exerted antagonistic effects on the BAT[64]. UCP1 content and PGC1α content was decreased in the BAT of exercised animals, relative to the control animals[64]. Furthermore, the oxidative capacity of BAT was decreased and adipocytes hypertrophied[64]. The explanation for this antagonistic regulation is that exercise, in itself, is thermogenic. Therefore, non-shivering thermogenesis from BAT is not required for thermoregulation and thus the tissue becomes less active[64]. Instead, the recruitment of beige fat is adapted as a compensatory reserve for thermogenesis, moving energy-dissipation away from core areas of the body[23,64]. Wu et al. also assessed the effects of diet on exercise-induced browning[64]. HF-feeding led to an enlargement in the area of Sc Ing adipocytes and drastically reduced UCP1 content[64]. Exercise reversed these effects, allowing the WAT adipocytes to display a similar morphology to that of the exercising low-fat fed animals. However, these outcomes did not significantly enhance the palmitate oxidation in the Sc Ing fat of the HF fed, exercising group relative to their sedentary counterparts[64]. Similar to exercise, diet was also regulated differently by the BAT[64]. In fact, HF-sedentary animals had significantly higher UCP1 and PGC1α contents as well as palmitate oxidation[64]. In this context, BAT plays a tremendous role in the regulation of energy balance[64]. This process is also known as diet-induced thermogenesis[64].

Because of the increase in energy expenditure, the activation and recruitment of thermogenic BAT has been widely proposed as a therapeutic tool for the treatment of obesity and insulin-resistance[23,63].

2.2.8. Diet-Induced Thermogenesis

As described previously, UCP1-mediated thermogenesis is not limited to thermoregulation and cold tolerance. Similar thermogenic mechanisms play an important role in the regulation of energy balance in diet-induced obesity (DIO)[66]. After a single meal, several circulating messengers travel to the brain to increase sympathetic stimulation to BAT[18]. These signals consist of insulin and glucose, as well as cholecystokinin, which is released from the stomach during a meal, and enterostatin, a pentapeptide that is released following the activation of pancreatic lipase[18]. These signals act on several hypothalamic nuclei, including the ventromedial nucleus (VMN) which was the first to be discovered and plays a crucial role in activating BAT[67]. The VMN has steroidogenic-factor 1 neurons projecting to autonomic centers that sympathetically activate BAT[67]. VMN also increases BAT thermogenesis through its stimulation of other hypothalamic areas that regulate autonomic output[67]. In DIO, the dorsomedial nucleus (DMN) of the hypothalamus is crucial for energy homeostasis and the activation of BAT thermogenesis[37]. Leptin is released from WAT[35,36] as an indication of fat storage in the body, and stimulates leptin receptors in the DMN to regulate sympathetic outflow through the raphe pallidus to the BAT[37]. This mechanism serves to counter the development of obesity[18]. Therefore, beyond thermoregulation, BAT is also highly influential in the regulation of energy balance under conditions of energy surplus[68]. This was demonstrated by Feldman and colleagues who studied the effects of UCP1-ablation on DIT[68]. They found that the expected increase in weight in mice on the obesogenic diet was even more pronounced in the absence of UCP1[68]. Surprisingly, UCP1-ablation led to the development of obesity in the standard

chow (SC) fed animals as well[68]. The researchers attributed this dramatic increase in mass to the enhanced metabolic efficiency of these UCP1-ablated mice[68]. Metabolic inefficiency is caused by diet-induced thermogenesis, or the increase in oxygen consumption due to the improved sensitivity to adrenergic stimulation in BAT[68]. UCP1-ablation eliminated DIT and, thus, the metabolic inefficiency in the HF fed mice[68]. In contrast, the HF fed, wild-type mice displayed an accelerated thermogenic response[68]. The enhanced metabolic response in these mice was met by a four-fold increase in UCP1 content relative to the wild-type controls[68]. Thus, these researches posited that norepinephrine-stimulated, diet-induced thermogenesis is largely dependent on UCP1 activity[68].

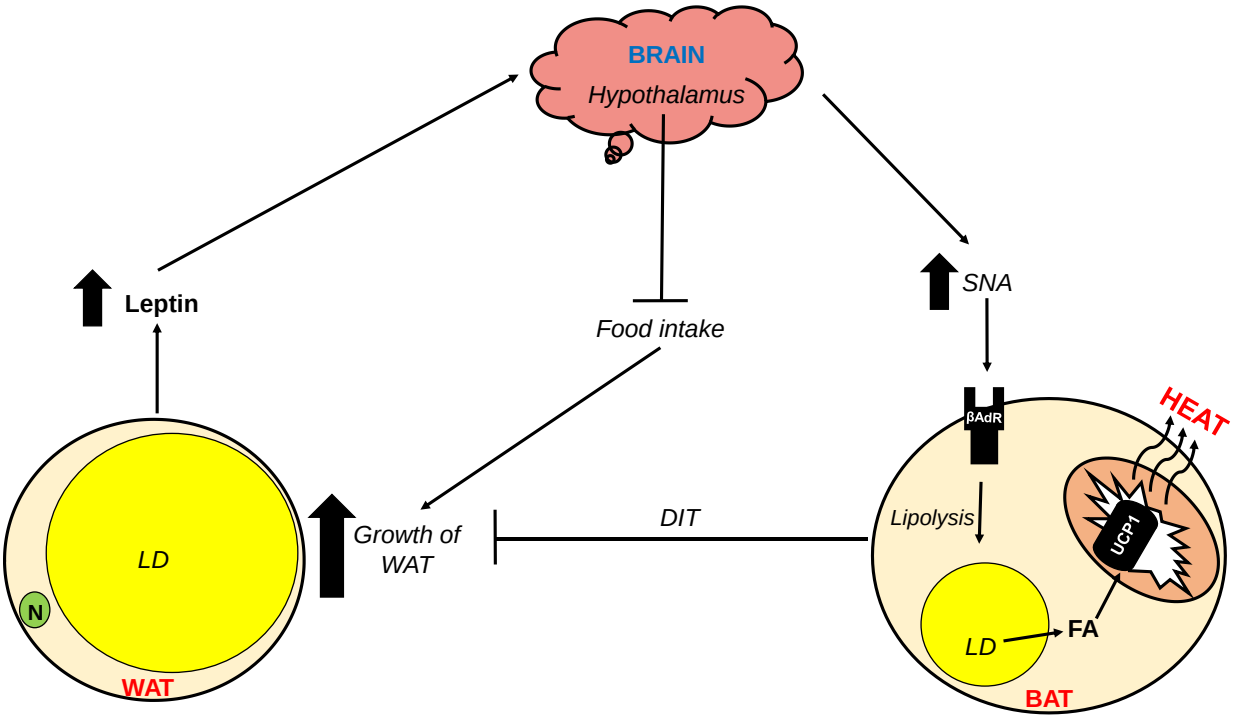

Fig. 6: Schematic representation of leptin-stimulated diet-induced thermogenesis (DIT). The diet-induced growth of adipose tissue is accompanied by an increase in leptin release from white-adipose tissue (WAT). Leptin binds to receptors in the hypothalamus, stimulating sympathetic output to the brown adipose tissue (BAT). At the level of the BAT, lipolysis is initiated, releasing free fatty acids (FFA) that bind to and activate UCP1 and thermogenesis. This mechanism counters the continued growth of WAT by compensating for the diet-induced disruption in energy balance. Leptin also reduces appetite to decrease food intake and attenuate fat accumulation. N, nucleus.

2.2.9. Chronic Obesity and Implications for BAT

The literature indicates that DIT is not sustainable under conditions of chronic HF-feeding, as we see in DIO[69]. This is compatible with the persistent growth in WAT mass seen in individuals on a high-fat diet (HFD)[69]. So et al. found that HF-feeding in rats caused a transient increase in heat production and whole-body energy expenditure that is sustained for two weeks[69]. Thereafter, heat production and energy expenditure was not different from that of control animals, and lead to a shift in energy balance that allows fat mass to grow[69]. In addition, these researchers found that ambulatory activity decreased gradually in the HF animals after the first two weeks of the diet, counteracting the initial burst in energy expenditure[69]. The authors suggested that the reduction in energy expenditure could, in part, be explained by the development of leptin resistance[69]. Leptin is released proportionally to WAT and is highly influential in the regulation of energy intake and non-exercise activity thermogenesis (NEAT)[69]. Accordingly, the HF animals had elevated plasma leptin, which is indicative of leptin resistance[69]. The reduction in energy expenditure, ambulatory activity and the consumption of a HFD combine to promote the growth of WAT and the progression of obesity[69].

At the level of the BAT, obesity also impacts energy dissipation[41]. Leitner et al demonstrated this by assessing BAT volume and metabolic activity in lean and obese subjects[41]. Following five hours of cold exposure, the subjects were injected with F-labelled fluorodeoxyglucose (F-FDG) and scanned using positron emission tomography/computed tomography (PET/CT) to determine the volume of six BAT depots and the glucose uptake occurring in each[41]. They found that obese subjects have a higher volume of BAT relative to the lean subjects. Interestingly, the obese subjects still activated less BAT than the healthy participants[41], which further reinforces the notion of DIO having a negative effect on the energy dissipating mechanisms of BAT.

The obesity-induced reduction in BAT function is also known as "whitening" of the brown fat, whereby BAT adapts the structural and functional characteristics of WAT[70]. Under conditions of obesity, it has been suggested that the dysfunction of BAT is initiated by the development of vascular rarefaction[70]. Brown adipocytes are typically highly vascularized for the reception of oxygen and nutrients and the delivery of heat to the rest of the body[42]. In fact, browning is characterized by increased vascularization of adipose tissue[71]. However, under conditions of DIO, high levels of intracellular fatty acids inhibit β-adrenergic signaling, which is crucial for the expression of vascular endothelial growth factor (VEGF)[70]. Consequently, the reduction in VEGF leads to a decrease in capillary density and the development of hypoxia[70]. What ensues is an increase in mitochondrial dysfunction, reactive oxygen species (ROS) production and mitochondrial membrane depolarization which, in turn, promotes the cellular removal of these organelles in a process known as mitophagy[70]. The loss of UCP1-containing mitochondria facilitates the deposition of lipids in these cells and the development of a more unilocular appearance[70]. In combination, these morphological and molecular adaptations are what facilitate the "whitening" of the brown adipocytes[70]. Shimizu et al. studied diet-induced "whitening" of BAT by examining brown adipocyte function in animals consuming a high-fat, high-sucrose diet. They observed reductions in *Ucp1* and *Pgc1α* transcript expression levels in these animals that was accompanied by a reduction in BAT vascularization[71]. In VEGF knock-out (KO) animals, they found that the resulting hypoxia led to reductions in β_1- and β_3-AdR content and suppressed PKA-mediated lipolysis[71]. Furthermore, the BAT mitochondria from these animals produced more ROS and displayed markers of mitophagy to a greater extent[71]. At the whole-body level, glucose and thermogenesis were impaired[71]. In this context, DIO-induced reduction of VEGF stimulates hypoxia in the BAT, which precedes whitening and mitochondrial dysfunction[71].

Although the aforementioned studies idenitified the diet-induced dysfunction of BAT, the molecular details underlying BAT-mediated mitochondrial uncoupling in DIO are still largely unknown. Leitner et al. used glucose uptake as a measure of BAT activity but did not consider heat production or DIT in their subjects. Furthermore, Shimizu et al. studied the effects of hypoxia on whitening and β-adrenergic signaling in BAT but did not assess whether this was having an impact on FA oxidation within the brown adipocytes. They also observed whole-body insulin resistance but did not investigate insulin-mediated glucose uptake in the BAT itself. Therefore, the purpose of our study is to measure FA and glucose oxidation in BAT under conditions of DIO to determine whether DIT is active. This will provide insight into potential oxidative mechanisms that are implicated under conditions of DIO and whether the tissue shifts its metabolism to preferentially oxidize glucose or FAs. This study will also investigate how BAT handles the excess substrate that is available under conditions of DIO and will provide novel insights into the lipogenic and lipolytic activity of this tissue in an obesogenic model. Understanding the implicated metabolic pathways is of tremendous importance for addressing the implicated molecular mechanisms in BAT-mediated DIT and carries great potential for the therapeutic management of obesity and related metabolic disorders.

3. Rationale, Objectives & Hypotheses

Based on previously published studies in animals[64,69] and humans[41,72], it is evident that BAT function is significantly altered under conditions of DIO. There is evidence of tissue enlargement and increased UCP1 content in BAT under DIO conditions in rats[64,69] and that UCP1 ablation abolishes diet-induced thermogenesis (DIT) and causes obesity in mice living at thermoneutrality[68]. In fact, it has also been proposed that BAT enhances its thermogenic activity when food is abundantly available[73,74]. Such adaptive mechanism would operate to limit weight gain and maintain body weight relatively stable over time. However, despite evidence of BAT enlargement and increased UCP1 content, great expansion of adiposity still occurs in DIO[64,69]. Furthermore, it has been reported that cold-induced BAT recruitment is much lower in obese than lean humans[41]. In this context, the contribution of BAT to DIT and its ability to prevent the development of obesity under conditions of chronic energy surplus remain controversial. Additionally, the physiological and molecular mechanisms by which DIO regulates BAT thermogenesis are still poorly understood.

Therefore, the objectives of this study are threefold:

1. To determine if UCP1-mediated mitochondrial uncoupling is indeed enhanced to promote thermogenesis under conditions of energy surplus and DIO.
2. To determine if DIO affects the ability of brown adipocytes to utilize glucose and fatty acids for thermogenesis.
3. To investigate the molecular and metabolic mechanisms underlying the adaptive thermogenic responses of BAT to DIO.

I hypothesize that:

1. DIO enhances glucose and fatty acid oxidation in BAT adipocytes due to increased UCP1-mediated uncoupled respiration.
2. DIO up-regulates the molecular machinery involved in the regulation of glucose and fatty acid uptake to increase the supply of substrate for thermogenesis.
3. The molecular machinery involved in TG recycling (lipolysis/re-esterification) is enhanced due to increased substrate influx into BAT adipocytes and high thermogenic demand in DIO.

4. Statement of Labour

All experiments described in this thesis were conducted primarily be D.D.E. Due to the logistics of these experiments, additional assistance was obtained from Shailee Jani, a current PhD student in Dr. Rolando Ceddia's lab. Shailee's contributions included tissue extraction, assisting with the performance of primary adipocyte metabolism assays and performing thin-layer chromatography (TLC).

Dr. Rolando Ceddia is the principle investigator and supervisor for this research study. All of the work conducted for this thesis was funded by a grant provided by the Natural Sciences and Engineering Research Council of Canada (NSERC).

5. Manuscript

High-fat diet enhances triglyceride recycling, impairs UCP1-mediated thermogenic activity, and causes insulin resistance in rat brown adipocytes

Daniel P. Da Eira, Shailee Jani, Rolando B. Ceddia

Muscle Health Research Center, School of Kinesiology and Health Science, York University, Toronto, Ontario, M3P 1J3, Canada

Running head: *Diet-induced obesity and brown adipose tissue thermogenesis*

To whom correspondence should be addressed:

Prof. Rolando B. Ceddia

Muscle Health Research Centre, School of Kinesiology and Health Science

York University, 4700 Keele St., North York, Ontario, M3J 13P, Canada.

Tel.: 416-736-2100 (Ext. 77204); Fax: 416-736-5774

E-mail: roceddia@yorku.ca

Abstract

Brown adipose tissue (BAT) is rich in uncoupling protein 1 (UCP1) and dissipates energy through thermogenesis. However, even though BAT mass and its UCP1 content increase under conditions of diet-induced obesity (DIO), marked expansion of the WAT is not prevented, suggesting impairment of BAT-mediated diet-induced thermogenesis (DIT) in obesity. Thus, the objective of this study was to investigate the metabolic and molecular mechanisms that regulated BAT thermogenesis in DIO. To accomplish this, rats were fed a high-fat diet (HFD) for eight weeks. Subsequently, glucose and fat metabolism and the molecular mechanisms underlying these processes were assessed in BAT adipocytes. Despite increasing BAT mass (1.3-fold), UCP1 content (2.1-fold), and isoproterenol (Iso)-induced lipolysis (1.6-fold), HFD reduced UCP1-mediated glucose (62%) and fatty acid (57%) oxidation, and abrogated insulin-stimulated glucose uptake in BAT adipocytes. Furthermore, phosphoenolpyruvate carboxykinase (PEPCK) and glycerol kinase (GyK) contents, as well as glycerol and palmitate incorporation into lipids were all significantly increased (1.8-fold, 2.1-fold, 2-fold, and 1.7-fold, respectively) in HFD BAT. This coincided with 3.6- and 3.7-fold elevations in lipoprotein lipase (LPL) and cluster of differentiation 36 (CD36), respectively, in HFD BAT adipocytes. Morphological analysis also revealed that these adipocytes were more unilocular in appearance. Altogether, these findings provide novel evidence that HFD suppresses UCP1-mediated thermogenesis, shifts metabolism toward triglyceride recycling, and induces insulin resistance in BAT adipocytes. These adaptive responses to chronic HFD are consistent with a mechanism that attenuates the contribution of BAT to DIT and favors the development of obesity and its related metabolic disorders.

Key words: Diet-induced thermogenesis, obesity, mitochondria uncoupling, glucose oxidation, PEPCK, PGC1α.

Introduction

Obesity is a rapidly growing global epidemic that is associated with several comorbidities including cardiovascular disease, cancer and Type II diabetes[1,2]. Besides being a major concern to public health, obesity also poses a great economic burden for the health care system[1]. In this context, research has focused on developing strategies to combat the development of obesity. Recently, adipose tissue and its ability to store and dissipate energy has sparked great interest as a potential therapeutic tool for the management of obesity and related metabolic disorders. In general, there are two main forms of adipose tissue: white and brown. White adipose tissue (WAT) is highly specialized to store fatty acids and glucose as triglycerides (TG) and release it under conditions of energy demand[12,23]. The adipocytes that compose this tissue are unilocular in appearance, with a large lipid droplet occupying the majority of the volume of the cell[12]. The second form of adipose tissue is brown adipose tissue (BAT). Brown adipocytes are typically multilocular in appearance with several small lipid droplets[12,23]. Unlike WAT, this tissue is also rich in mitochondria that contain uncoupling protein-1 (UCP1), which uncouples electron transport from oxidative phosphorylation resulting in the production of heat in a process known as thermogenesis[18].

The activation of BAT UCP1 has been studied classically under conditions of cold-exposure. Cold-exposure activates the sympathetic nervous system (SNS) and the release of norepinephrine (NE) in BAT[18]. The binding of NE to beta-adrenergic receptors on the brown adipocytes initiates lipolysis within the cells and increases the release of fatty acids (FAs) from intracellular TG[18]. The binding of these FAs to UCP1 is what promotes mitochondrial uncoupling and thermogenesis in BAT[18,58]. Cold-induced activation of BAT has produced promising results

for the management of obesity[16]. In fact, Sepa-Kishi et al. showed that cold-acclimation reduced WAT mass in rats despite an increase in food intake[16].

Interestingly, BAT can also be activated under conditions of diet-induced obesity (DIO) where the stimulus is a WAT-derived hormone known as leptin[35,36]. Similar to cold-exposure, leptin enhances sympathetic nerve activity, lipolysis and UCP1-mediated thermogenesis in BAT[37]. In this context, the dissipation of energy is known as diet-induced thermogenesis (DIT) and serves to maintain energy homeostasis within the organism and prevent the growth of adipose tissue[18]..

However, based on previously published studies in animals[64,69] and humans[41,72], it is evident that BAT function is significantly altered under conditions of DIO. There is evidence of tissue enlargement and increased UCP1 content in BAT under DIO conditions in rats[64,69] and that UCP1 ablation abolishes diet-induced thermogenesis (DIT) and causes obesity in mice living at thermoneutrality[68]. In fact, it has also been proposed that BAT enhances its thermogenic activity when food is abundantly available[73,74]. Such adaptive mechanism would operate to limit weight gain and maintain body weight relatively stable over time. However, despite evidence of BAT enlargement and increased UCP1 content, great expansion of adiposity still occurs in DIO[64,69]. Furthermore, it has been reported that cold-induced BAT recruitment is much lower in obese than lean humans[41]. In this context, the contribution of BAT to DIT and its ability to prevent the development of obesity under conditions of chronic energy surplus remain controversial. Additionally, the physiological and molecular mechanisms by which DIO regulates BAT thermogenesis are still poorly understood. Therefore, the objective of this study was to investigate the molecular and metabolic mechanisms that regulate BAT DIT under conditions of DIO. We hypothesized that DIO would increase DIT due to enhanced UCP1-mediated mitochondrial uncoupling. To address this, we fed rats a high-fat diet (HFD) for eight weeks. Subsequently,

glucose and fat metabolism and the molecular mechanisms underlying these processes were assessed in isolated BAT adipocytes. Here, we show that although there was an increase in UCP1 content, HFD suppressed BAT DIT, increased TG recycling and caused insulin resistance in rat brown adipocytes.

Materials and Methods

Reagents — Type II collagenase, isoproterenol, FA-free bovine serum albumin (BSA), palmitic acid, and the free glycerol determination kit was purchased from Sigma (St. Louis, MO, USA). Oligomycin was purchased from Cayman Chemical (Ann Arbor, MI, USA). [1-^{14}C] palmitic acid and [^{14}C(U)] glycerol and D-[U-^{14}C] glucose were purchased from American Radiolabeled Chemicals (St. Louis, MO, USA). The lactate assay kit was from BioVision (Milpitas, CA). Protease (cOmplete Ultra Tablets) and phosphatase (PhosSTOP) inhibitors were obtained from Roche Diagnostics GmbH (Mannheim, Germany). The β-actin (Cat # 4067), tyrosine hydroxylase (TH; cat. no. 2792), adipose triglyceride lipase (ATGL; cat. no. 2138), hormone-sensitive lipase (HSL; cat. no. 4107), and $pHSL_{Ser660}$ (cat. no. 4126) antibodies were purchased from Cell Signaling (Danvers, MA, USA). The β_3-adrenergic receptor (β_3-AdR, Cat # sc-50436) and Glucose transporter type 4 (GLUT4, Cat # sc-7938) antibodies were purchased from Santa Cruz Biotechnology (Dallas, TX, USA). The carnitine palmitoyltransferase 1B (CPT1B, Cat # PB9491) antibody was purchased from BosterBio (Pleasanton, CA, USA). Glucose transporter type 1 (GLUT1, Cat # ab115730), glycerol kinase (GYK) (Cat # ab180525), phosphoenolpyruvate carboxykinase cytoplasmic (PEPCK-C, Cat # ab28455), and UCP1 (Cat # ab23841) were purchased from Abcam (Toronto, ON, Canada). The peroxisome proliferator-activated receptor gamma coactivator-1α (PGC-1α, Cat # AB3242) antibody was purchased from Millipore (Temecula, CA, USA).

Animals and diet – Male albino rats (Wistar strain) at approximately 250g were housed at 22°C on a 12/12-h light/dark cycle. These rats were assigned to either a standard laboratory chow (SC) diet (27% protein, 13% fat and 60% carbohydrates from Lab Diet Cat #5012) group or a high-fat (HF) diet (20% protein, 60% fat, 20% carbohydrates from Research Diets, Cat # D12492) group and

were fed *ad libitum* for 8 weeks. After 8 weeks of feeding, animals were anesthetized and tissues were harvested for experiments. The protocol containing all animal procedures described in this proposal were specifically approved by the Committee on the Ethics of Animal Experiments of York University (York University Animal Care Committee, YUACC, permit number 2016-5) and performed strictly in accordance with the YUACC guidelines. All surgeries were performed under ketamine/xylazine anesthesia, and all efforts were made to minimize suffering.

Adipose tissue morphology - Morphological analysis of iBAT was performed using light microscopy as described previously[64,75]. Briefly, a sample (~50–100 mg) of each fat tissue was collected and fixed in 4% paraformaldehyde, 0.1 M phosphate-buffered saline (PBS), pH 7.4, for 24h at room temperature. Following fixation, adipose tissue samples were washed three times in PBS and stored at 4°C in 70% ethanol. Samples were then embedded in paraffin blocks, sectioned, and stained with hematoxylin and eosin (H & E). Digital images of tissue sections were captured with a Nikon Eclipse Ti (Nikon Canada, Mississauga, ON, Canada) under X20 and X40 magnification.

Body weight and fat mass – Changes in body weight were measured by comparing weekly weight recordings to a baseline measurement. Interscapular brown adipose tissue (iBAT), aortic BAT (aBAT), subcutaneous inguinal (Sc Ing), and epididymal (Epid) fat pads were extracted, trimmed of any non-fat tissue, and individually weighed.

Brown adipose tissue extraction and adipocyte isolation – iBAT and aBAT were extracted and carefully trimmed of any muscle, connective tissue, and white fat and used for adipocyte isolation as previously described[76]. iBAT and aBAT were combined to maximize the yield of brown adipocytes. The tissues were initially incubated in Krebs-Ringer bicarbonate HEPES buffer

(KRBH) prepared fresh on the day of each experiment from stock solutions of salts and buffers (stored at 4°C) to give the following final concentrations: 120 mM NaCl, 4.8 mM KCl, 2.5 mM CaCl2, 1.2 mM KH_2PO_4, 1.2 mM $MgSO_4$, 15 mM $NaHCO_3$, 30 mM HEPES, and type II collagenase (0.83 mg/ml). The tissues were incubated at 37°C under orbital agitation (120 orbital strokes/min) for 5 min. Subsequently, the combined tissues were vortexed for 5s and filtered, with the filtrate being discarded. The remaining tissues were finely minced and incubated in fresh KRBH-4% BSA containing collagenase (0.83 mg/ml) at 37°C under orbital agitation (120 orbital strokes/min) for about 20 – 30 min. The digested tissue was then strained using a nylon mesh and isolated cells were transferred to plastic tubes, washed 3 times, and resuspended in KRBH containing 3.5% FA free BSA (KRBH-3.5% BSA). In order to distribute an equal number of adipocytes in each treatment condition, cell diameters were measured and total cell counts were determined[77].

Glucose and palmitate oxidation – Glucose and palmitate oxidation as a measure of oxidative capacity were assessed by $^{14}CO_2$ release in isolated BAT adipocytes ($5x10^5$ cells) as previously described[75]. Adipocytes were incubated in KRBH-3.5% BSA containing either 0.2 μCi/ml of [1-^{14}C] palmitic acid and 200 μM non-labelled palmitate, or 0.2 μCi/ml of D-[U-^{14}C] glucose and 5.5 mM non-labeled D-glucose for 1h. To examine the effect of lipolysis on substrate oxidation, the β-agonist isoproterenol (Iso, 100 nM) was added to the media. To distinguish substrate oxidation for ATP production (coupled respiration) from UCP1-mediated proton leak (uncoupled respiration), the ATP Synthase inhibitor oligomycin (Oligo) was added to cells 15 min prior to the incubation without or with Iso. Following the 1h incubation period, the media were acidified using 0.2 ml of H_2SO_4 (5N) and kept sealed for one additional hour for the release and collection of $^{14}CO_2$ from the cells and media. The incubation vials were prepared with a centered well containing

a filter paper that was moistened with 0.2 ml of 2-phenylethylamine/methanol (1:1, vol:vol) for the capture of $^{14}CO_2$. At the end of the incubation, the filter paper was removed from the well and placed in scintillation fluid for radioactive counting[27,78].

Lipolysis – Lipolysis was measured in isolated BAT adipocytes ($7.5x10^5$ cells) either under basal or Iso-stimulated (100 nM) conditions. Each assay was conducted in triplicates and samples were incubated for 75 min at 37°C with gentle shaking (50 orbital strokes/min). Following the incubation, a 200 µl aliquot of the incubation medium was extracted from each vial for the determination of glycerol concentration.

Glycerol and Palmitate incorporation into lipids – Glycerol and Palmitate incorporation into lipids were measured using isolated BAT adipocytes ($5x10^5$ cells). Adipocytes were incubated in KRBH-3.5% BSA containing 0.2 µCi/ml of [^{14}C(U)] glycerol for 1h. Subsequently, lipid extraction took place according to the method of Dole and Meinertz[79] and counted for radioactivity[78]. Palmitate incorporation into lipids was measured in isolated BAT adipocytes ($5x10^5$ cells) incubated in KRBH-3.5% BSA containing 0.2 µCi/ml of [1-^{14}C] palmitic acid and 200 µM non-labelled palmitate for 1h. Lipids were extracted from these adipocytes using the Folch's method[80], dried under nitrogen, and resuspended in 50 µl of chloroform:methanol (2:1, v:v). Four µl of sample and TG standard (triolein, Nu-chek Prep Inc., Minnesota, USA) were spotted 2 cm above the lower edge of silica coated flexible polyester thin layer chromatography plates (20 cm x 20 cm) (Whatman, Maidstone, United Kingdom). Lipids were separated using a hexane–diethyl ether–acetic acid (70:30:1, v:v:v) solvent and then exposed to iodine vapor for visualization. After the evaporation of iodine, the spots adjacent to the standard, corresponding to TG, were scraped off the plate and counted for radioactivity.

Glucose Uptake – Isolated adipocytes were used to determine glucose uptake as described previously[81]. Briefly, adipocytes were resuspended in glucose-free KRB containing HEPES (30 mM; KRB-HEPES) and 1% BSA, pH 7.4. Subsequently, $4x10^5$ cells were transferred to plastic tubes and incubated at 37°C for 1h. Insulin (100 nM) was added for the final 20 min of the incubation period. Subsequently, KRB-HEPES containing 0.5 mM 2-deoxy-D-glucose and 0.5 μCi of 2-[1,2-^{3}H]deoxy-D-glucose was added to the cells for 3 min, and the incubations were terminated by the addition of cytochalasin B (1.5 mM stock solution). Aliquots of cell suspension (240 μl) were quickly placed in plastic microtubes containing 100 μl of di-"isononyl" phthalate. The tubes were centrifuged for 30s (6000 × g) to separate cells from the radioactive incubation medium. Subsequently, fat cells were collected by cutting the tubes through the oil phase and transferred to scintillation vials to be counted for radioactivity. Nonspecific transport was determined in the same conditions, except that cytochalasin B (50 μM final concentration) was added to the medium before the addition of cells. Nonspecific values were subtracted from all conditions.

Measurement of Lactate Production – Lactate production was measured using a commercially-available kit as per the manufacturer's instructions. Briefly, cells were isolated as previously described and incubated in KRBH-3.5% BSA for 75 min. Following incubation, an aliquot of media was extracted and stored at -80°C until analysis.

RNA isolation and quantitative PCR – BAT samples were flash frozen in liquid nitrogen and stored at -80°C until RNA isolation. RNA was then isolated using TRIzol™ (ThermoFisher Scientific, Waltham, MA, USA) and resuspended in sterile water. Complimentary DNA (cDNA) was made with 2 μg of RNA using ABM EasyScript™ Reverse Transcriptase cDNA Synthesis kit (Diamed, Mississauga, ON, Canada) as per the manufacturer's instructions. All primers that were used for

real- time PCR have been previously designed using the software PrimerQuest (IDT) based on probe sequences available at the Affymetrix database (NetAffx™ Analysis Centre, http://www.affymetrix.com/ analysis) for each given gene. Samples were run in duplicates on a 96-well plate. Each 20 µl reaction will contain 4 µl of cDNA, 0.4 µl of primer, 10 µl of Brightgreen 2x qPCR Mastermix (Diamed, Mississauga, ON, Canada) and 5.6 µl of RNA-free water. qPCR analysis was performed using a Bio-Rad CFX96 Real Time PCR Detection System (Bio-Rad, Mississauga, ON, Canada) using the following amplification conditions: 95°C (10 min); 40 cycles of 95°C (15 s), 65°C (1 min); a 0.5°C step-wise increment from 65°C to 95°C. All genes were normalized to the housekeeping-gene β-actin, and relative differences in gene expression between treatment groups were determined using the ΔΔCt method[82]. Values are presented as fold increases relative to the SC group. The primers to be used are as follows: Cluster of differentiation (Cd36) forward (ACGACTGCAGGTCAACATACTGGT), reverse (TGGTCCCAGTCTCATTTGCCACA); lipoprotein lipase (Lpl) forward (TTGAGAAAGGGCTCTGCCTGAGTT), reverse (TGCTTCTCTTGGCTCTGACCTTGT).

Western blotting – BAT samples were extracted from each rat, snap frozen in liquid nitrogen, and frozen at -80^{o}C for later use. Tissues were homogenized in buffer containing 25 mM Tris-HCl, 25 mM NaCl (pH 7.4), 1 mM $MgCl_2$, 2.7 mM KCl, 1% Triton-X and protease and phosphatase inhibitors (Roche Diagnostics GmbH, Mannheim, Germany). Following centrifugation of the homogenates, the infranatant was collected. An aliquot of each sample was used in a Bradford assay to determine protein concentration. The samples were then diluted 1:1 with 2x Laemli sample buffer and incubated at 95°C for 5 min. Twenty-five µg of protein from each sample was loaded on to gels and subject to SDS-PAGE, transferred to a PVDF membrane, and probed with

the antibody of interest. The antibody dilutions were 1:1000 and the loading control was β-actin. Densitometry analysis was conducted using the Scion Image program.

Statistical Analysis – Statistical analyses were conducted by using either unpaired t-tests or ANOVAs with the Bonferroni post-hoc comparison using the GraphPad Prism statistical analysis program. Statistical significance was set at $p<0.05$. Error bars are ±SEM.

Results

Effects of HF-feeding on body weight and fat mass – In order to confirm that the HFD was causing obesity in the animals, we measured weight gain relative to baseline and adipose tissue mass. The weight gained in weeks 1 – 3 was not statistically significantly different between the two groups, although the average weight gained in the HFD group was higher in each of these weeks. After week 4, the weight gained in the HFD group was significantly higher than in the SC animals (188.6 g ± 8.2 *vs*. 127.8 g ± 12.3 respectively) (Fig. 7A). This difference in weight gain persisted until the end of the study. After the eighth and final week of feeding, the weight gained by the HFD group was 1.5-fold higher than in the SC animals. Interestingly, the differences in weight gained in weeks five to six and six to seven in the SC animals were not statistically significant. In contrast, the HFD animals demonstrated persistent increments in weight gain throughout the entire study. This suggests that the stagnation in weight gain that the control animals experienced was overcome in the HFD group. Differences in weight gain can be attributed to the enhanced growth of WAT in the HFD animals. There was a 2-fold increase in the Sc Ing fat and a 2.4-fold increase in the Epid fat of the HFD animals (Fig. 7B). Interestingly, the growth of WAT was accompanied by an increase in BAT mass. iBAT and aBAT masses were increased 1.3- and 1.4-fold, respectively, in the HFD animals (Fig. 7C).

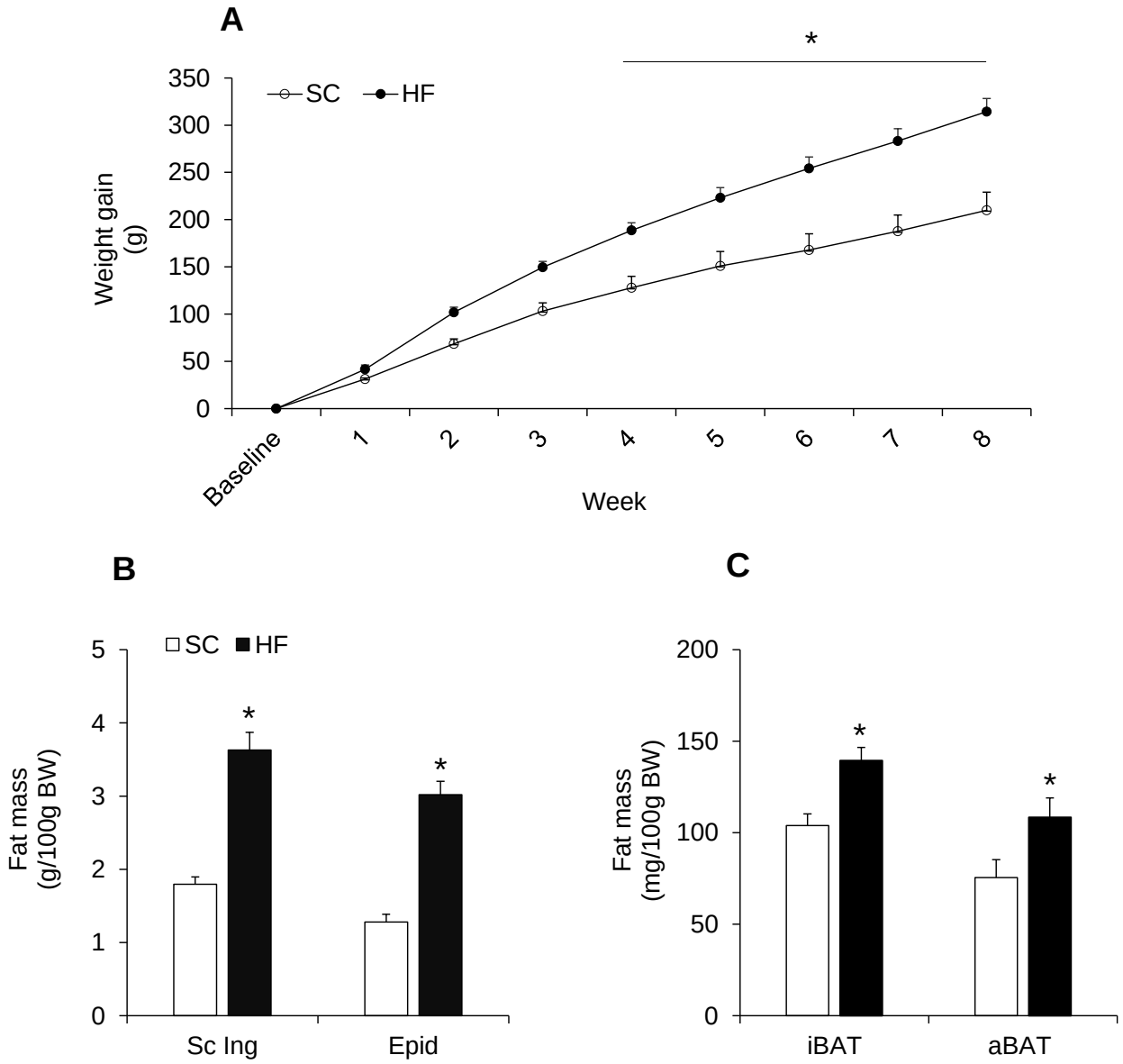

Fig. 7: Weight gain was significantly enhanced in the HF animals in weeks 4-8 of the diet (A). The difference in weight gain is likely attributable to the diet-induced increase in subcutaneous inguinal (Sc Ing) and epididymal (Epid) fat masses (B). This was met by an increase in iBAT and aBAT masses (C). *$p<0.05$ *vs*. SC. Repeated measures two-way ANOVA was used to compare groups/time, except for fat mass where a t-test was used. *n* = 10-17 rats.

Effects of HF-feeding on PGC1α, CPT1B and UCP1 contents: After observing an increase in BAT mass, it was important to determine whether this was accompanied by an increase in thermogenic machinery. Animals in the HFD group exhibited a 1.6-fold increase in PGC1α protein content (Fig. 8A), a 17.5-fold increase in CPT1B content (Fig. 8B) and a 2.1-fold increase in UCP1 content, relative to the control group (Fig. 8C). Taken together, these results suggest that the molecular machinery necessary for oxidation and thermogenesis were enhanced in BAT under conditions of DIO.

Effects of oligomycin and Iso on palmitate oxidation in the BAT of HF-fed animals- We then wanted to determine whether the increased expression of thermogenic proteins was altering substrate oxidation. Palmitate oxidation was measured as an indication of thermogenic capacity in the BAT. We measured this under four conditions: Basal, Iso, Oligo and Iso+Oligo. Under basal conditions, palmitate oxidation did not differ between the SC group and the HF group (Fig. 8D). Incubation with Oligo significantly increased palmitate oxidation 2.7-fold in the BAT of the SC animals but did not alter oxidation in the BAT of the HF animals (Fig. 8D). From these findings, we concluded that mitochondrial uncoupling accounts for the majority, if not all, of the palmitate being oxidized in the BAT of standard chow (SC)-fed control animals. However, when we compare SC and HFD groups, the difference in Oligo-induced palmitate oxidation is striking. In fact, palmitate oxidation was 57% lower in BAT adipocytes from HFD animals than controls (Fig. 8D). Furthermore, when incubated with both Iso and Oligo, palmitate oxidation was reduced by 44% in the brown adipocytes of the HF group (Fig. 8D), although this was not statistically significant. Thus, we clearly demonstrated an impairment in UCP1-mediated palmitate oxidation under conditions of HF-feeding. Interestingly, Iso-stimulated palmitate oxidation in the BAT of SC animals, in the absence or presence of Oligo, is significantly lower than palmitate oxidation

with Oligo alone (Fig. 8D), which suggests that Iso is having a suppressive effect on palmitate oxidation.

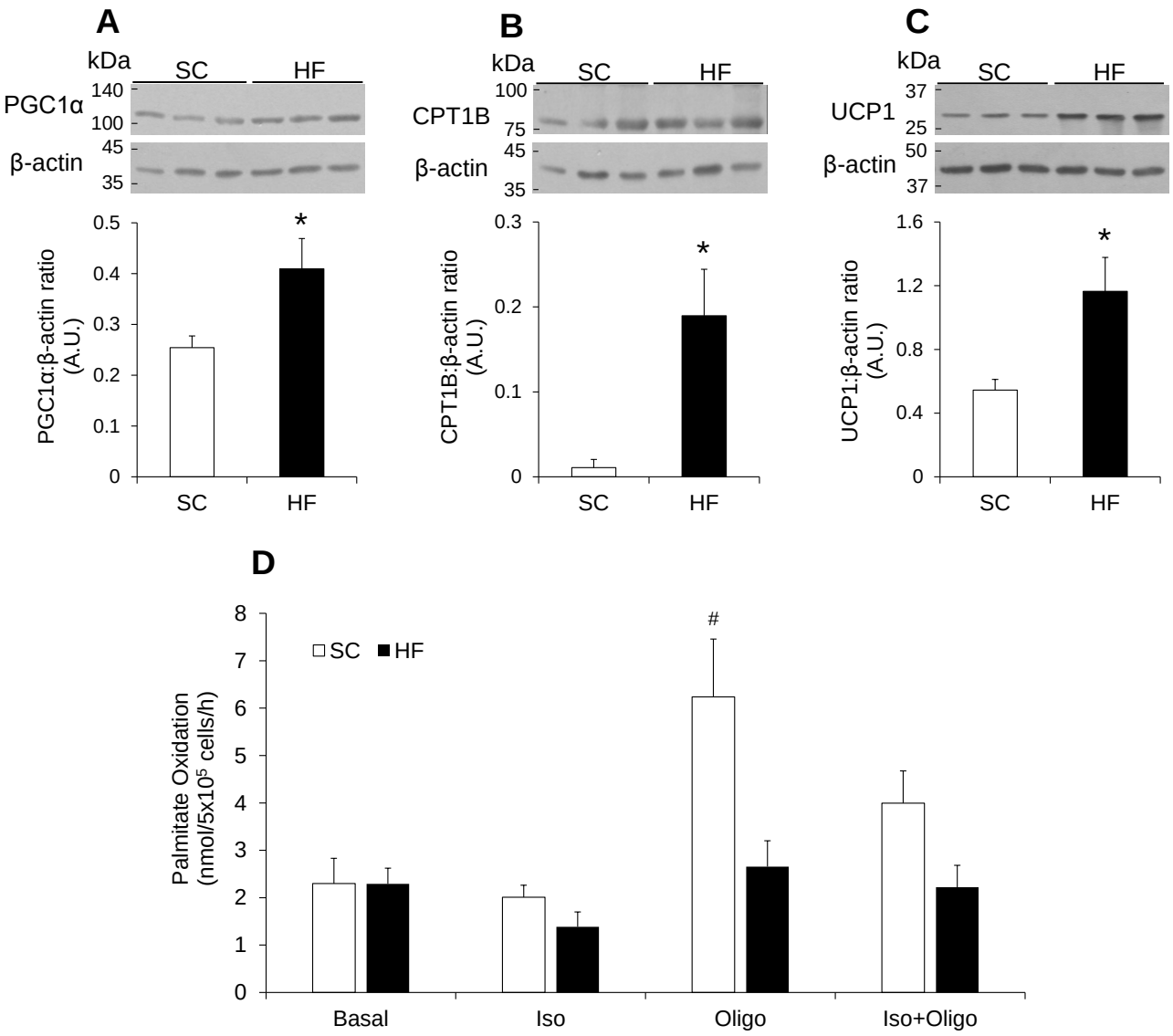

Fig. 8: HF-feeding increased PGC1α, CPT1B and UCP1 contents in the iBAT (A, B and C, respectively). However, the increased expression of thermogenic proteins did not elicit an enhanced thermogenic response. There was no significant difference in basal or isoproterenol (Iso)-stimulated palmitate oxidation between the SC and HF groups. Iso-stimulated palmitate oxidation seemed to be suppressed in the HFD animals in the absence or presence of Oligo. Furthermore, HF-feeding significantly reduced oligomycin (Oligo)-induced palmitate oxidation (D). A.U., arbitrary units. *$p<0.05$ *vs*. SC. $^{\#}p<0.05$ *vs*. HF Oligo, SC Basal, SC Iso, SC Iso+Oligo. Two-way ANOVA was used to compare groups/conditions except for PGC1α, CPT1B and UCP1 contents where t-tests were used. *n* = 4-15 rats for A-C. *n* = 10-14 rats for D.

Effects of HFD on Lpl and CD36 gene expression in BAT: We considered that FA uptake could be a limiting factor for palmitate oxidation in the BAT of the HFD animals. As an indication of the adipocytes' FA import capacity, we measured gene expression for FA uptake machinery. *Lpl* (Fig. 9A) and *Cd36* (Fig. 9B) gene expressions were enhanced 3.6- and 3.7-fold in the BAT of the HF animals, respectively. These findings suggest that FA import is enhanced, rather than impaired, under conditions of HF-feeding and that an alternative mechanism is contributing to the reduction in palmitate oxidation.

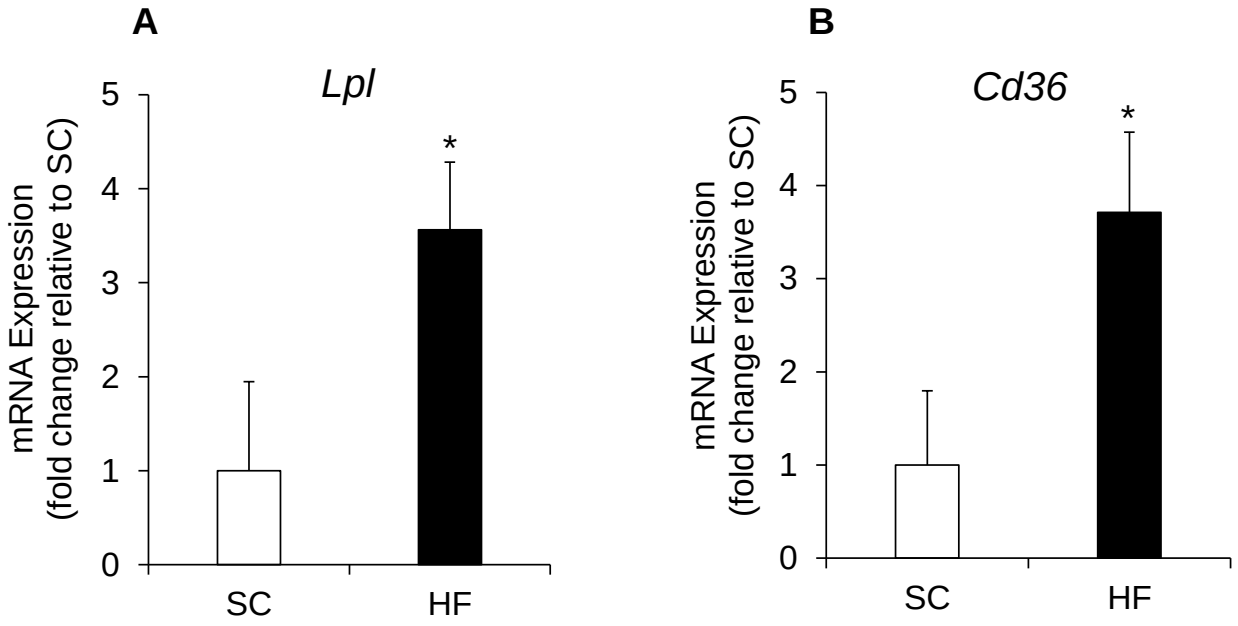

Fig. 9: HF-feeding increased *Lpl* and *Cd36* gene expressions in the BAT (A and B, respectively). *p<0.05 *vs.* SC. T-tests were used to compare groups. *n*= 10-11 rats.

Effects of oligomycin and Iso on glucose oxidation in the BAT of HF-fed animals- HF-feeding suppressed glucose oxidation in the BAT (Fig. 10). Basal glucose oxidation was reduced 48% in the BAT of the HF animals (Fig. 10). Similarly, Iso-stimulated glucose oxidation decreased 49 and 56% in the HF group in the absence and presence of Oligo, respectively (Fig 10). Relative to basal measures, incubation with Oligo did not reduce glucose oxidation (Fig. 10), which suggests that

mitochondrial uncoupling accounts for the majority of the glucose being oxidized in both groups. However, our data show that mitochondrial uncoupling was impaired under conditions of DIO. Oligo-induced glucose oxidation was 62% lower in the BAT of the HF animals (Fig. 10), relative to the SC animals, indicating that there is a suppression in UCP1-mediated glucose oxidation under conditions of DIO.

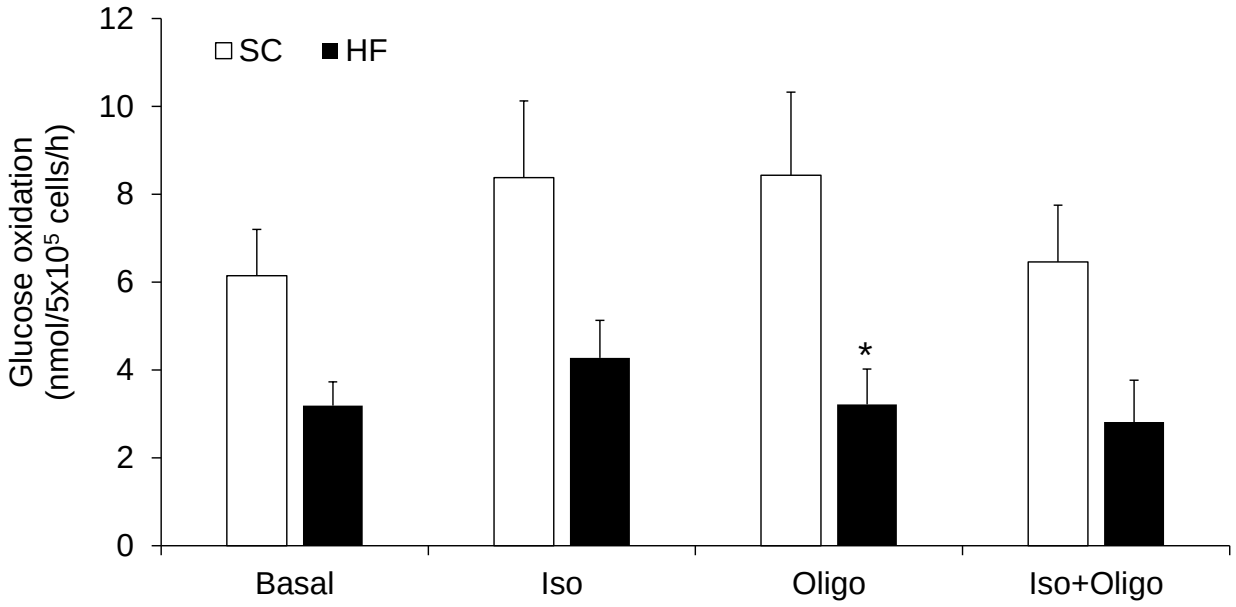

Fig. 10: HF-feeding impaired glucose oxidation and significantly reduced Oligo-induced glucose oxidation in BAT adipocytes. *p<0.05 *vs.* SC. Two-way ANOVA was used to compare groups/conditions. *n* = 10-14 rats.

Effects of HF-feeding on GLUT1 and GLUT4 protein contents and glucose uptake in isolated brown adipocytes – HFD increased GLUT1 protein content ~25-fold but did not alter GLUT4 content in iBAT (Fig. 11A and 11B, respectively). Importantly, the measure of GLUT4 content did not differentiate between cytosolic and membrane-bound forms of the protein. Therefore, we could not assess if HFD impaired GLUT4 translocation in iBAT adipocytes. However, we did measure glucose uptake in isolated iBAT adipocytes to assess whether HFD impaired the ability

of these cells to transport glucose under basal and insulin-stimulate conditions. We found that basal glucose uptake did not differ between HFD and SC animals. However, in the presence of insulin, SC adipocytes displayed a 2-fold increase in glucose uptake, whereas the HFD adipocytes did not respond to the hormone at all (Fig. 11C). In fact, insulin-stimulated glucose uptake was severely impaired in the BAT of HFD animals, revealing a 78% reduction relative to the SC group. In conclusion, BAT developed insulin resistance (IR) under DIO conditions.

Effects of HFD on lactate production in isolated brown adipocytes – Lactate production was measured in isolated adipocytes under basal conditions. The HFD animals produced 2.7-fold more lactate than the SC animals. This result suggests that BAT metabolism shifted to glycolysis under conditions of DIO (Fig. 11D).

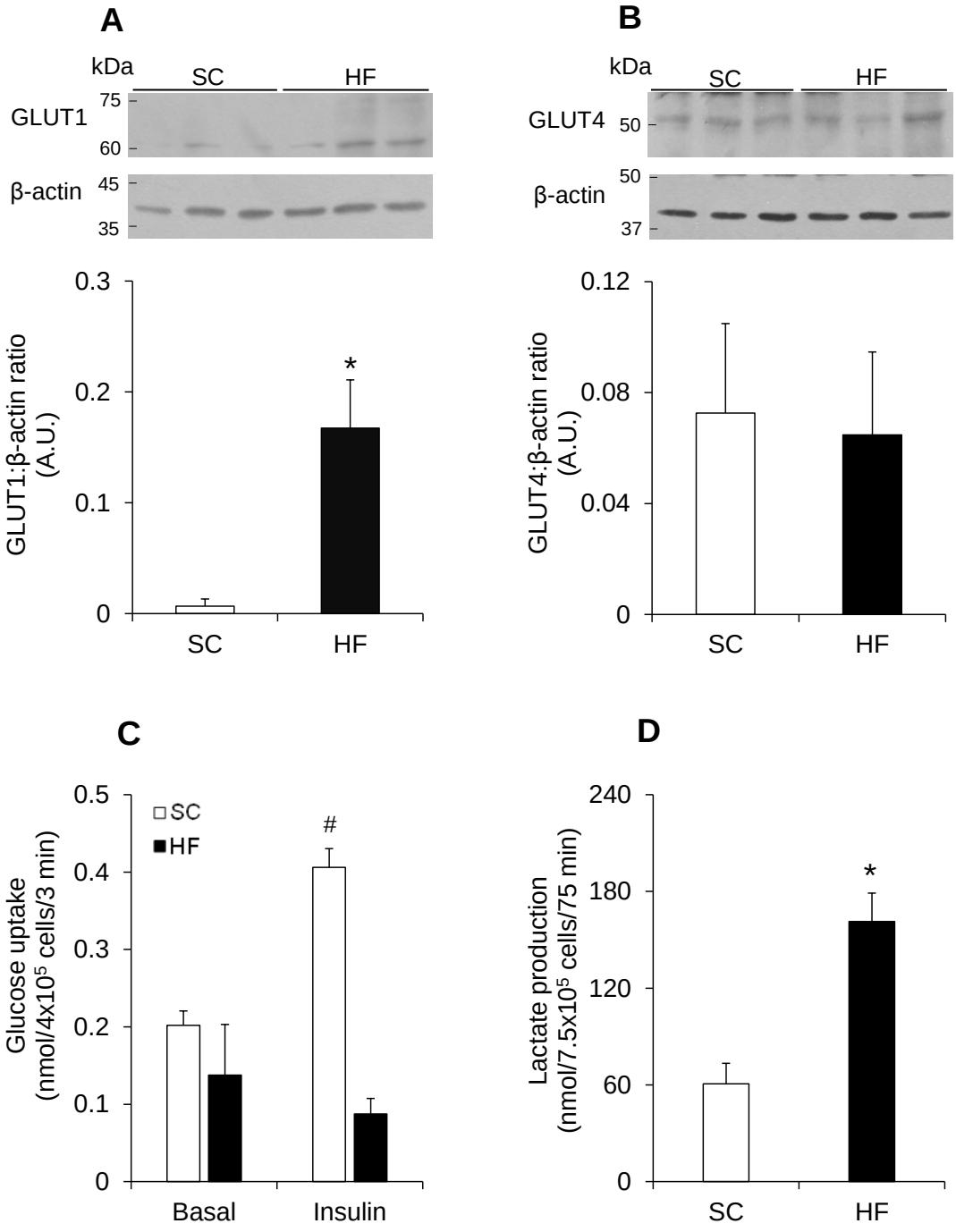

Fig. 11: HF-feeding increased GLUT1 protein content but did not change GLUT4 protein content (A and B, respectively). Under basal conditions, glucose uptake was comparable between the SC and HFD groups (C). However, BAT insulin-stimulated glucose uptake was shown to be significantly impaired with HF-feeding (C). Lactate production was enhanced in BAT under conditions of DIO (D). *$p<0.05$ *vs*. SC. $^{\#}p<0.05$ *vs*. SC Basal, HF Insulin. t-tests were used to compare groups except for glucose uptake (C) where a Two-way ANOVA was used to compare groups/conditions. *n* = 4-5 for A-B. *n* = 5-9 for C-D.

Effects of a HFD on glycerol and palmitate incorporation into TAG and PEPCK and GyK content in brown adipocytes – HFD enhanced *g*lycerol and palmitate incorporation into lipids 2- (Fig. 12C) and 1.7-fold (Fig. 12D), respectively in the BAT. This was supported by a 1.8-fold increase in PEPCK protein content (Fig. 12A) and a 2.1-fold increase in GyK protein content (Fig. 12B). In concert, these mechanisms favored the synthesis of TG.

Effect of a HFD on adipocyte morphology – Under control conditions, brown adipocytes are multilocular in appearance (Fig. 13A). Following the consumption of a HFD, these adipocytes undergo morphological adaptations where they become more unilocular in appearance (Fig. 13B).

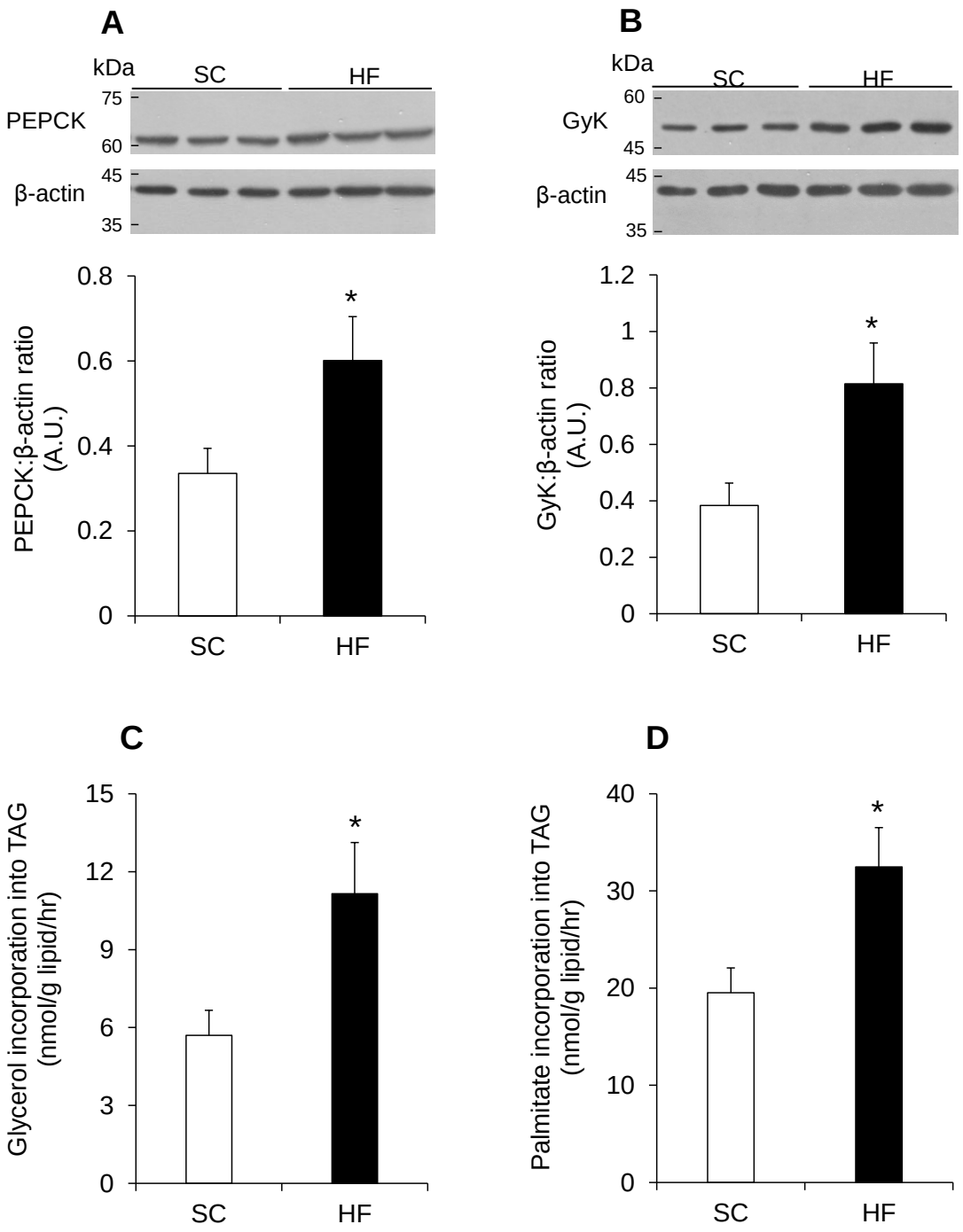

Fig. 12: HF-feeding increased PEPCK (A) and GyK (B) contents in the BAT. This was accompanied by an increase in glycerol and palmitate incorporation into TAG (C and D, respectively). *p<0.05 *vs*. SC. t-tests were used to compare groups. *N* = 8–15 rats for A–B. *n* = 6–9 rats for C-D.

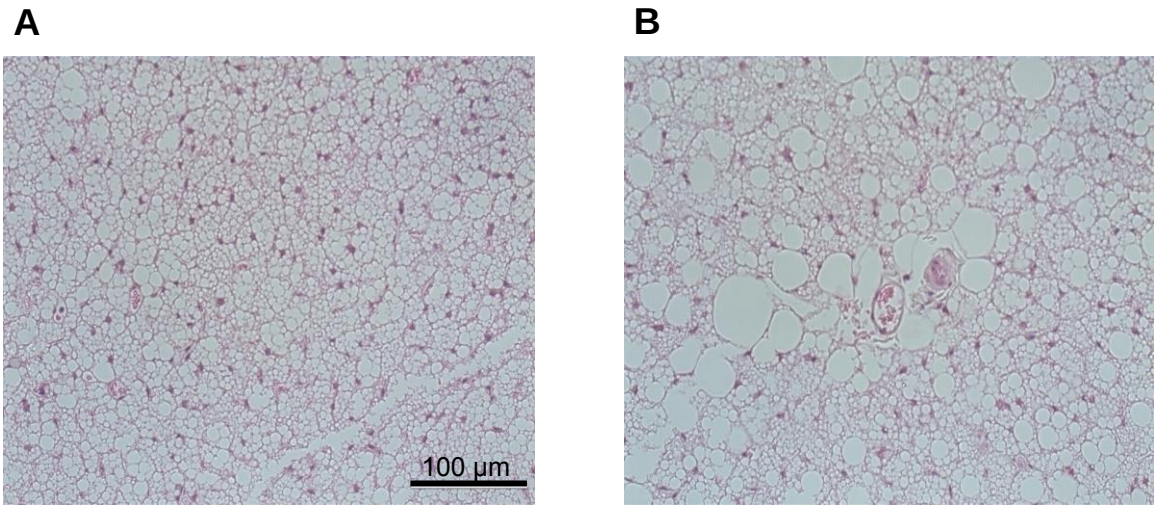

Fig. 13: Microscopic image of iBAT using H&E staining. Viewed at 40x magnification. In the SC animals, the brown adipocytes were more multilocular in appearance. HFD induced a morphological adaptation in these adipocytes, making them appear more unilocular.

Effects of HF-feeding on lipolysis and β3-AdR, TyHy, ATGL and pHSL contents in the BAT – Basal lipolysis was reduced by 70% in the BAT of HF animals relative to the SC group, although the difference was not statistically significant (Fig. 14A). Western blot analysis revealed 84 and 27% reductions in Tyrosine hydroxylase (TyHy) and ATGL contents, respectively (Fig. 14B and 14D, respectively). HSL_{660} phosphorylation was increased under conditions of HF-feeding, although this was not statistically significant (Fig. 14E). Under Iso-stimulated conditions, lipolysis was enhanced 1.6-fold in the BAT of the HF animals (Fig. 14A). This was supported by the 6.1-fold increase in β3-AdR content in this group (Fig. 14C).

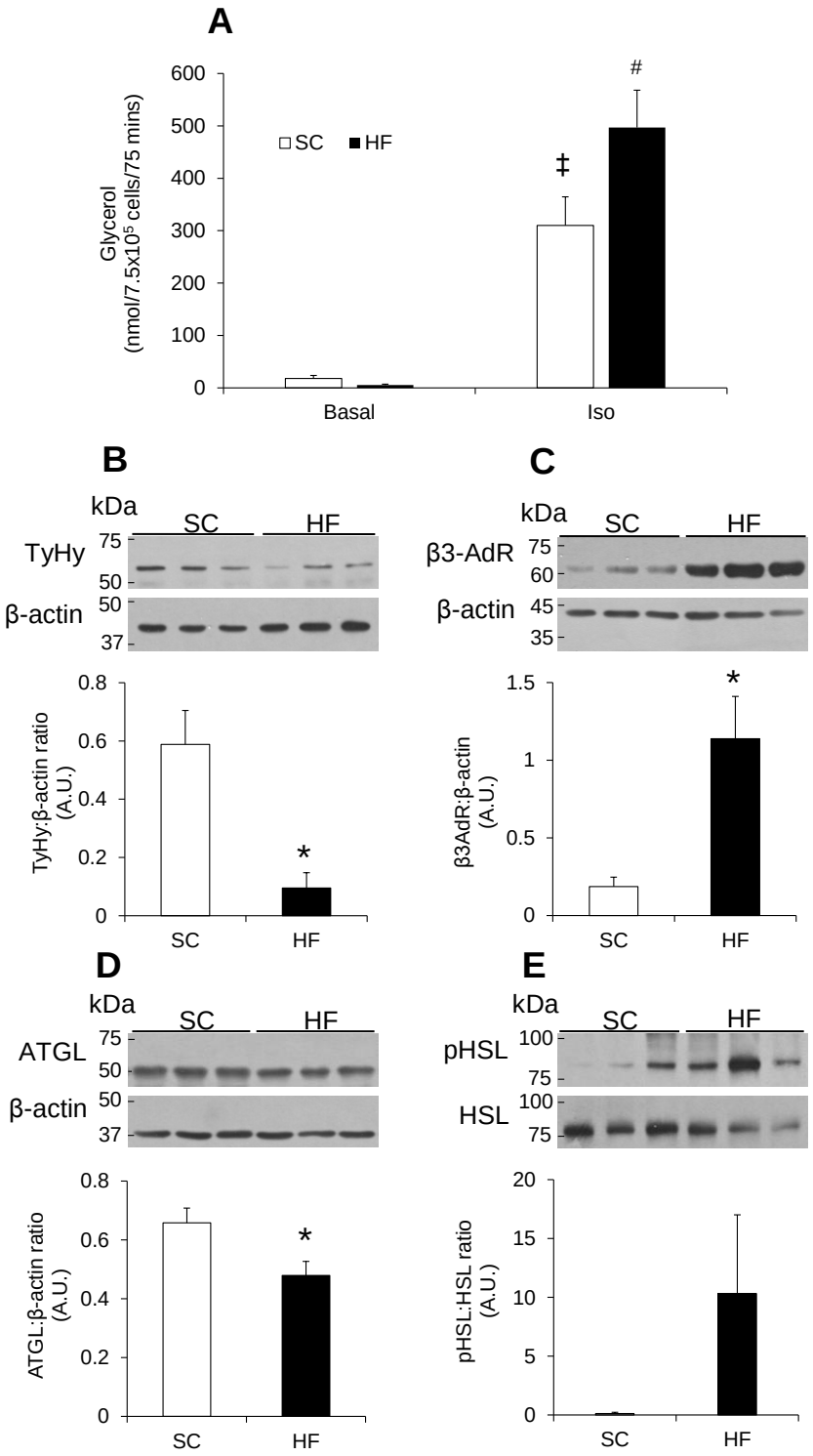

Fig. 14: HFD enhanced Iso-stimulated lipolysis but did not alter basal lipolysis (A). Accordingly, TyHy content was reduced in the BAT of HF-fed animals (B). This was compensated for by an increase in β3-AdR content (C). Furthermore, ATGL content was reduced and pHSL was unaltered in the BAT of HF animals (D and E, respectively). *$p<0.05$ *vs*. SC. $^{‡}p<0.05$ *vs*. SC Basal. $^{\#}p<0.05$ *vs*. HF Basal, SC Iso. t-tests were used to compare groups except for Lipolysis (A) where a Two-way ANOVA was used to compare groups/conditions. *n* = 6-8 for A. *n* = 4-5 rats for B-E.

Discussion

Our study provides novel evidence indicating that the recruitment of BAT mass and thermogenic proteins is insufficient to increase mitochondrial uncoupling and DIT under conditions of chronic obesity. Instead, UCP1-mediated thermogenesis is impaired and BAT develops the functional and morphological characteristics of WAT.

We were surprised to find that both palmitate and glucose oxidation were impaired with HF-feeding. As mentioned previously, we studied substrate oxidation in brown adipocytes under four conditions: Basal, Iso, Oligo and Iso+Oligo. Basal palmitate oxidation was not different between the two groups. Interestingly, we observed a marked difference in palmitate oxidation following an incubation of our cells with the ATP Synthase inhibitor, Oligo. As expected, Oligo-induced palmitate oxidation was not significantly different from basal oxidation. This is because mitochondrial uncoupling accounts for the majority of the palmitate being oxidized in BAT[16]. However, despite the increase in UCP1 content in the BAT of the HF animals, Oligo-induced palmitate oxidation was significantly lower in comparison to what was seen in the SC animals. In this context, we can conclude that mitochondrial uncoupling is impaired under conditions of DIO. Thus, our original hypothesis is rejected. A possible explanation for this is that lipolysis is severely impaired, limiting the activation of UCP1 in the BAT[18]. In accordance with our hypothesis, we demonstrated decreases in TyHy and ATGL protein contents. These molecular adaptations likely originate from the diminishing sympathetic output from the hypothalamus as a result of diet-induced leptin resistance[69]. When we stimulated the cells with an exogenous β-agonist (Iso), we observed an enhanced lipolytic response in the BAT of the HF animals. This was supported by a 6.1-fold increase in β3-AdR protein content. The overexpression of β3-AdR is likely a

compensatory mechanism employed by the cell to maximize adrenergic activation, although, *in vivo*, it is futile given the impaired production of NE.

Surprisingly, Iso-stimulation did not produce the expected increase in palmitate oxidation. In theory, the increased expression of CPT1B in the BAT of the HF animals should have facilitated the import of lipolysis-derived FAs into the mitochondria[34], which is known to promote the activation of UCP1 and FA oxidation[16,18]. A plausible explanation for this discrepancy is that lipolysis-derived FA were redirected to TG synthesis rather than UCP1 activation[16]. In support of this, we found elevated levels of CD36 and LPL, to promote the reuptake of released FAs into the cell, and 2 and 1.7-fold increases in glycerol and palmitate incorporation into lipids, respectively. The recycling of lipolysis-derived glycerol is facilitated by the increased expression of GyK. However, the majority of the glycerol used for TG esterification is derived from the diet-induced increase in PEPCK content[60]. The drive to store FAs as TG is likely an adaptive response, *in vivo*, to suppressed levels of lipolysis and UCP1 activity and the overabundance of dietary substrate. Acute stimulation with a β-agonist was clearly not enough to override this. However, it is intriguing to consider whether chronic stimulation, following the consumption of a HFD, could reverse these effects and re-brown the whitened brown fat[16]. In this context, our second and third hypotheses are confirmed; FA and glucose are processed and stored as TAG in the BAT of HF-fed animals. However, contrary to our hypotheses, these mechanisms do not serve to fuel BAT thermogenesis.

The concept of TG re-esterification was demonstrated recently by Sepa-Kishi et al in the beige fat of cold-acclimated animals[16]. In their study, the elevated rate of TG synthesis was met by an accelerated rate of lipolysis, producing an energy-consuming cycle that likely contributed to decrease WAT mass and conferred a multilocular appearance to the white adipocytes[16]. In our

study we found a similar increase in TG synthesis, but no change in lipolysis. In this context, the rate of TG turnover was reduced, favouring the growth of the lipid droplets in the brown adipocytes. Taken together, the attenuations in Oligo and Iso-stimulated palmitate oxidation indicate that UCP1 activity and DIT are compromised in the BAT under conditions of DIO, making the HF animals more metabolically efficient[68] and prone to increasing their fat mass.

Another factor contributing to the reduction in palmitate oxidation is respiratory chain dysfunction. Under basal conditions, proton flow from the mitochondrial intermembrane space to the matrix is partitioned through UCP1 and ATP Synthase[57]. Therefore, when ATP Synthase is inhibited with Oligo, the proton flux through UCP1 is increased, producing a burst in UCP1-mediated palmitate oxidation. This response was observed in the BAT of the SC animals and is indicative of a recruitable thermogenic reserve in this tissue. In contrast, when brown adipocytes from HF animals were incubated with Oligo, palmitate oxidation did not change. This suggests that oxidation is already exclusively mediated by UCP1 and devoid of ATP Synthase activity. Based on these findings, we can conclude that HF-feeding suppresses respiratory chain activity and oxidative phosphorylation in brown adipocytes. Diet-induced alterations to mitochondrial function have been reported by other researchers, including Shimizu et al., who found that obesity-induced hypoxia in the BAT of mice promotes the formation of reactive oxygen species and the onset of mitochondrial dysfunction[71]. Furthermore, it is plausible to consider that the reduction in ATP Synthase activity seen in brown adipocytes from HFD animals is a consequence of mitophagy and lower mitochondrial content[71], which explains the shift to glycolysis in these cells. However, this warrants further investigation.

Similar to palmitate oxidation, glucose oxidation was also consistently lower in the BAT of the HF animals under all incubation conditions (Basal, Iso, Oligo, Iso+Oligo), reaching

significance with Oligo. We measured GLUT1 and GLUT4 protein expression to eliminate transport as a limiting factor for glucose metabolism and found that GLUT1 content increased 24.9-fold and GLUT4 did not significantly change. However, the measure of GLUT4 did not differentiate between cytosolic and membrane-bound GLUT4 and was, therefore, not a good representative measure of insulin-stimulated glucose uptake[5]. We therefore ran a glucose uptake assay to measure basal and insulin-stimulated glucose import. When stimulated with insulin, there was an expected increase in glucose uptake in the brown adipocytes of SC animals, however, there was no change in the brown adipocytes of HF animals. Furthermore, when comparing the two groups to each other, there was a 78% reduction in insulin-stimulated glucose uptake in the HF animals. Similar findings were reported by Lapa et al. who found that insulin-stimulated glucose uptake was severely impaired in a rat model of Type II diabetes[83]. Therefore, it is evident that chronic HF-feeding causes the BAT to develop IR. Under basal conditions, this difference between the two groups was not evident. This is likely due to the overexpression of GLUT1 in this tissue, which compensated for the reduction in basal GLUT4-mediated glucose uptake. However, this mechanism is evidently limited in its capacity to compensate for the impairment in insulin-stimulated glucose uptake, as was demonstrated in the brown adipocytes from the HF animals.

It was then important for us to consider the fate of the glucose being imported under basal conditions. Because glucose oxidation is suppressed, we hypothesized that this glucose was entering the glycolytic pathway and being converted to lactate, rather than pyruvate[46]. Accordingly, we demonstrated a 2.7-fold increase in lactate production in the BAT of the HF animals, confirming our hypothesis. Hypoxia is known to develop in the brown adipocytes of HF-fed animals[71]. This is compatible with a shift to anaerobic glucose metabolism and an enhanced production of lactate[46]. Glycolysis-derived lactate is used as a substrate for glyceroneogenesis[84],

further promoting the synthesis of TG and the growth of intracellular lipid droplets in the brown adipocytes

In conclusion, although there is an increase in the content of oxidative proteins, palmitate and glucose oxidation are significantly reduced in the BAT of HF-fed animals. Instead, FAs are used for TG synthesis and storage. The deposition of lipids in this tissue is further promoted by the diet-induced attenuation of lipolysis. The subsequent hypertrophy of these adipocytes confers a more unilocular appearance to the cells. Furthermore, this tissue develops insulin resistance and loses its ability to contribute to glucose clearance from the circulation, which exacerbates the metabolic complications imposed by the diet. Together, these functional and structural adaptations make the BAT appear and function more like WAT. The process of conversion is known as whitening[70]. These adaptations are compatible with the increase in fat mass and enhanced capacity to gain weight. Understanding the molecular mechanisms that are impacted in the BAT under conditions of DIO provides us with metabolic targets for therapeutic management of obesity and insulin resistance.

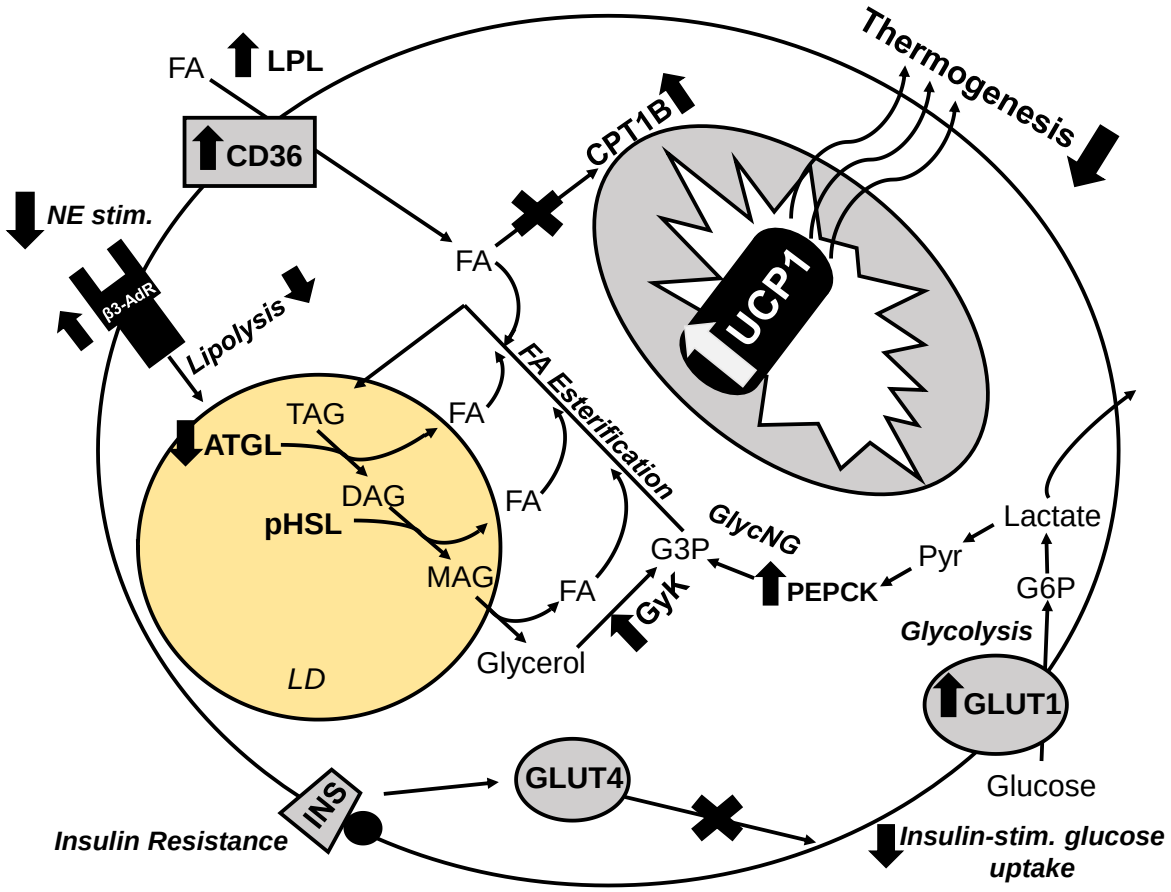

Fig. 15: Despite the increases in carnitine palmitoyltransferase-1B (CPT1B) and Uncoupling protein-1 (UCP1) in the brown adipose tissue (BAT) of high-fat (HF)-fed animals, relative to controls, mitochondrial uncoupling is impaired. Instead, fatty acids (FAs) are being diverted to triacylglycerol (TG) synthesis in the cell. TG formation is supported by the increases in glycerol kinase (GyK) and phosphoenolpyruvate carboxykinase (PEPCK) contents, which provide the glycerol-3-phosphate (G3P) necessary for FA esterification, and FA uptake which is supported by the increased expression of cluster differentiation 36 (CD36) and lipoprotein lipase (LPL). Norephinephrine (NE)-stimulated lipolysis is limited due to the reduction of catecholamine synthesis and adipose triglyceride lipase (ATGL) content. This can contribute to the reduced activation of UCP1. Basal glucose uptake is preserved due to the increase in glucose transporter 1 (GLUT1) protein content. The glucose that is imported in to the cell is diverted to glycolysis and lactate production is enhanced. Accordingly, there is a reduction in glucose oxidation. Insulin-stimulated glucose uptake is suppressed, indicating the development of insulin resistance in BAT under conditions of HF-feeding. GLUT4, glucose transporter isoform 4; INS, insulin receptor; pHSL, phosphorylated HSL; β-AdR, β-adrenergic receptor; LD, lipid droplet; DAG, diacylglycerol; MAG, monoacylglycerol; GlycNG, glyceroneogenesis; Pyr, pyruvate. X indicates suppression of a pathway. Arrows indicate flow through a pathway.

6. Future Directions

In this study, we provide evidence that DIT is suppressed under conditions of DIO. However, little is known regarding the temporal progression of the involved metabolic adaptations in BAT. In this context, a future direction for this research is to measure diet-induced alterations in BAT mitochondrial uncoupling and substrate metabolism over the course of a HFD. So et al. reported a transient increase in whole-body energy expenditure that occurred in the first few days of HF feeding in rats, but was turned off as HF feeding continued[69]. Therefore, a time-dependent analysis of BAT thermogenesis particularly at early stages of HF-feeding may reveal novel information regarding the molecular mechanisms that lead to the inability of BAT to sustain a thermogenic response in the face of energy surplus.

Another potential future direction is studying BAT function under alternative dietary conditions. The diet we provided our HF animals with was high in fat and sucrose. However, it is relevant to consider whether a ketogenic diet would generate a different result with respect to BAT adaptations. Srivastava et al. fed mice a ketogenic diet and found that UCP1 content was enhanced in the BAT[85]. This was accompanied by an increase in ETC proteins. Therefore, I propose investigating BAT mitochondrial uncoupling under conditions of ketogenic feeding to determine whether substrate oxidation is altered under such conditions. Given the HF content of the diet, it is also important to investigate whether glucose disposal through UCP1-mediated uncoupling is enhanced in BAT by feeding a ketogenic diet.

These proposed future directions carry great impact for the understanding BAT function under different dietary conditions and is of tremendous importance for the development of therapeutic tools for the management of obesity and related metabolic disorders.

7. References

1. Monsey, M. S. & Gerhard, D. M. Obesity. Introduction. *Yale J. Biol. Med.* **87,** 97–8 (2014).

2. Blüher, M. Obesity : global epidemiology and pathogenesis. *Nat. Rev. Endocrinol.* **15,** 288–298 (2019).

3. Katzmarzyk, P. T. *et al.* International Study of Childhood Obesity, Lifestyle and the Environment (ISCOLE): Contributions to Understanding the Global Obesity Epidemic. *Nutrients* **11,** 1–24 (2019).

4. Ludwig, D. & Friedman, M. Increasing adiposity: consequence or cause of overeating? *JAMA* **311,** 2167–2168 (2014).

5. Czech, M. P., Tencerova, M., Pedersen, D. J. & Aouadi, M. Insulin signalling mechanisms for triacylglycerol storage. *Diabetologia* **56,** 949–964 (2013).

6. Templeman, N. M., Skovsø, S., Page, M. M., Lim, G. E. & Johnson, J. D. A causal role for hyperinsulinemia in obesity. *J. Endocrinol.* **232,** R173–R183 (2017).

7. Berry, R., Jeffery, E. & Rodeheffer, M. S. Weighing in on adipocyte precursors. *Cell Metab.* **19,** 8–20 (2014).

8. Poher, A. L., Altirriba, J., Veyrat-Durebex, C. & Rohner-Jeanrenaud, F. Brown adipose tissue activity as a target for the treatment of obesity/insulin resistance. *Front. Physiol.* **6,** 1–9 (2015).

9. Narayanaswami, V. & Dwoskin, L. P. Obesity: Current and Potential Pharmacotherapeutics and Targets. *Pharmacol Ther* **170,** 116–147 (2017).

10. Bray, G. A. & Ryan, D. H. Update on obesity pharmacotherapy. *Ann. New York Acad. Sci.* **1311,** 1–13 (2014).

11. Bazan, I. S. & Fares, W. H. Review of the Ongoing Story of Appetite Suppressants, Serotonin Pathway, and Pulmonary Vascular Disease. *Am. J. Cardiol.* **117,** 1691–1696

12. Cinti, S. Transdifferentiation properties of adipocytes in the adipose organ. *AJP Endocrinol. Metab.* **297,** E977–E986 (2009).

13. Cohen, P., Spiegelman, B. M. & Drubin, D. G. Cell biology of fat storage. *Mol Biol Cell* **27,** 2523–2527 (2016).

14. Sanchez-Gurmaches, J. & Guertin, D. A. Adipocyte Lineages : Tracing Back the Origins of Fat. *Biochim. Biophys. Acta* **1842,** 340–351 (2015).

15. Soler-Vázquez, M. C., Mera, P., Zagmutt, S., Serra, D. & Herrero, L. New approaches targeting brown adipose tissue transplantation as a therapy in obesity. *Biochem. Pharmacol.* **155,** 346–355 (2018).

16. Sepa-kishi, D. M., Jani, S., Da Eira, D. & Ceddia, R. B. Cold acclimation enhances UCP1 content, lipolysis, and triacylglycerol resynthesis, but not mitochondrial uncoupling and

fat oxidation, in rat white adipocytes. *Am J Physiol Cell Physiol* **316,** 365–376 (2019).

17. Mottillo, E. P. *et al.* Coupling of lipolysis and de novo lipogenesis in brown , beige , and white adipose tissues during chronic β3-adrenergic receptor activation. *J Lipid Res* **55,** 2276–2286 (2014).

18. Cannon, B. & Nedergaard, J. Brown Adipose Tissue: Function and Physiological Significance. *Physiol Rev* **84,** 277–359 (2004).

19. Inokuma, K. *et al.* Uncoupling Protein 1 Is Necessary for Norepinephrine-Induced Glucose Utilization in Brown Adipose Tissue. *Diabetes* **54,** 1385–1391 (2005).

20. Morigny, P., Houssier, M., Mouisel, E. & Langin, D. Adipocyte lipolysis and insulin resistance. *Biochimie* **125,** 259–266 (2016).

21. Oller Do Nascimento, C., Ribeiro, E. & Oyama, L. Metabolism and secretory function of white adipose tissue : effect of dietary fat. *Ann. Brazilian Acad. Sci.* **81,** 453–466 (2009).

22. Contreras, C. *et al.* The brain and brown fat. *Ann. Med.* **47,** 150–168 (2015).

23. Sepa-Kishi, D. M. & Ceddia, R. B. Exercise-Mediated Effects on White and Brown Adipose Tissue Plasticity and Metabolism. *Exerc. Sport Sci. Rev.* **44,** 37–44 (2016).

24. Zechner, R. *et al.* FAT SIGNALS - Lipases and Lipolysis in Lipid Metabolism and Signaling. *Cell Metab.* **15,** 279–291 (2012).

25. Bolsoni-Lopes, A. & Alonso-Vale, M. Lipolysis and lipases in white adipose tissue – An update. *Arch Endocrinol Metab* **59,** 335–342 (2015).

26. Gregoire, F. M., Smas, C. M. & Sul, H. E. I. S. Understanding Adipocyte Differentiation. *Physiol. Rev.* **78,** 783–809 (1998).

27. Gaidhu, M. P., Anthony, N. M., Patel, P., Hawke, T. J. & Ceddia, R. B. Dysregulation of lipolysis and lipid metabolism in visceral and subcutaneous adipocytes by high-fat diet : role of ATGL , HSL , and AMPK. *Am J Physiol Cell Physiol* **298,** 961–971 (2010).

28. Itani, S., Ruderman, N., Schmieder, F. & Boden, G. Lipid-Induced Insulin Resistance in Human Muscle Is Associated With Changes in Diacylglycerol, Protein Kinase C, and IkBa. *Diabetes* **51,** 2005–2011 (2002).

29. Saltiel, A. R. & Kahn, C. R. Insulin signalling and the regulation of glucose and lipid metabolism. *Nature* **414,** 799–806 (2001).

30. Taniguchi, C. M., Emanuelli, B. & Kahn, C. R. Critical nodes in signalling pathways: Insights into insulin action. *Nat. Rev. Mol. Cell Biol.* **7,** 85–96 (2006).

31. Leto, D. & Saltiel, A. R. Regulation of glucose transport by insulin : traffic control of GLUT4. *Nat. Rev. Mol. Cell Biol.* **13,** 383–396 (2012).

32. Weisberg, S. P. *et al.* Obesity is associated with macrophage accumulation. *J. Clin. Invest.* **112,** 1796–1808 (2003).

33. Uysal, K. T. & Wiesbrock, S. M. Protection from obesity- induced insulin resistance in mice lacking TNF- a function. *Nature* **389,** 610–614 (1997).

34. Boudina, S. & Graham, T. E. Mitochondrial function/dysfunction in white adipose tissue. *Exp. Physiol.* **99,** 1168–1178 (2014).

35. Haynes, W. G., Morgan, D. A., Walsh, S. A., Mark, A. L. & Sivitz, W. I. Receptor-mediated regional sympathetic nerve activation by leptin. *J. Clin. Invest.* **100,** 270–278 (1997).

36. Tartaglia, L. A. *et al.* Identification and expression cloning of a leptin receptor, OB-R. *Cell* **83,** 1263–1271 (1995).

37. Enriori, P. J., Sinnayah, P., Simonds, S. E., Rudaz, C. G. & Cowley, M. A. Leptin Action in the Dorsomedial Hypothalamus Increases Sympathetic Tone to Brown Adipose Tissue in Spite of Systemic Leptin Resistance. *J. Neurosci.* **31,** 12189–12197 (2011).

38. Kadowaki, T. *et al.* Adiponectin and adiponectin receptors in insulin resistance , diabetes , and the metabolic syndrome. *J. Clin. Invest.* **116,** 1784–1792 (2006).

39. Wei, Q. *et al.* Adiponectin is required for maintaining normal body temperature in a cold environment. *BMC Physiol.* **17,** 1–11 (2017).

40. Cohen, P. & Spiegelman, B. M. Brown and beige fat: Molecular parts of a thermogenic machine. *Diabetes* **64,** 2346–2351 (2015).

41. Leitner, B. P. *et al.* Mapping of human brown adipose tissue in lean and obese young men. *Proc. Natl. Acad. Sci. U. S. A.* **114,** 8649–8654 (2017).

42. Bargut, T. C. L., Aguila, M. B. & Mandarim-de-Lacerda, C. A. Brown adipose tissue: Updates in cellular and molecular biology. *Tissue Cell* **48,** 452–460 (2016).

43. Fredriksson, J. M. & Nedergaard, J. Norepinephrine Specifically Stimulates Ribonucleotide Reductase Subunit R2 Gene Expression in Proliferating Brown Adipocytes : Mediation via a cAMP / PKA Pathway Involving Src and Erk1 / 2 Kinases. *Exp. Cell Res.* **215,** 207–215 (2002).

44. Kompare, M. & Rizzo, W. B. Mitochondrial Fatty-Acid Oxidation Disorders. *Semin. Pediatr. Neurol.* **15,** 140–149 (2008).

45. Sokolov, S. S., Balakireva, A. V, Markova, O. V & Severin, F. F. Negative Feedback of Glycolysis and Oxidative Phosphorylation : Mechanisms of and Reasons for It. *Biochem.* **80,** 559–564 (2015).

46. Akram, M. Mini-review on Glycolysis and Cancer. *J Canc Educ* **28,** 454–457 (2013).

47. Liberti, M. V & Locasale, J. W. A new layer of glycolysis. *Nat. Chem. Biol.* **12,** 577 (2016).

48. Gray, L. R., Tompkins, S. C. & Taylor, E. B. Regulation of pyruvate metabolism and human disease. *Cell. Mol. Life. Sci.* **71,** 2577–2604 (2014).

49. Sharma, V. *et al.* Redox-induced activation of the proton pump in the respiratory complex I. *Proc. Natl. Acad. Sci.* **112,** 11571–11576 (2015).

50. Akram, M. Citric Acid Cycle and Role of its Intermediates in Metabolism. *Cell Biochem.*

Biophys. **68,** 475–478 (2014).

51. Yarian, C., Toroser, D. & Sohal, R. Aconitase is the main functional target of aging in the citric acid cycle of kidney mitochondria from mice. *Mech Ageing Dev* **127,** 79–84 (2006).

52. Eaton, S. *et al.* Mammalian mitochondrial β -oxidation. *Biochem J* **320,** 345–357 (1996).

53. Van Der Bliek, A. M., Sedensky, M. M. & Morgan, P. G. Cell biology of the mitochondrion. *Genetics* **207,** 843–871 (2017).

54. Papa, S. *et al.* in *Advances in Mitochondrial Medicine* (eds. Scatena, R., Bottoni, P. & Giardina, B.) 3–37 (Springer, 2012).

55. Nicholls, D. G. & Locke, R. M. Thermogenic mechanisms in brown fat. *Physiol Rev* **64,** 1–64 (1984).

56. Nedergaard, J. *et al.* UCP1: The only protein able to mediate adaptive non-shivering thermogenesis and metabolic inefficiency. *Biochim. Biophys. Acta - Bioenerg.* **1504,** 82–106 (2001).

57. Divakaruni, A. S. & Brand, M. D. The Regulation and Physiology of Mitochondrial Proton Leak. *Physiology* **26,** 192–205 (2011).

58. Fedorenko, A., Lishko, P. V. & Kirichok, Y. Mechanism of Fatty-Acid-Dependent UCP1 Uncoupling in Brown Fat Mitochondria. *Cell* **151,** 400–413 (2013).

59. Hanson, R. W. & Reshef, L. Glyceroneogenesis revisited. *Biochimie* **85,** 1199–1205 (2003).

60. Reshef, L. *et al.* Glyceroneogenesis and the Triglyceride / Fatty Acid Cycle *. *J Biol Chem* **278,** 30413–30416 (2003).

61. Kaslow, R. Regulation of glycogen synthase in muscle and adipose tissue during fasting and refeeding. *Am J Physiol* **254,** 720–725 (1988).

62. Kristin I. Stanford, Roeland J.W. Middelbeek, Kristy L. Townsend, D. A., Eva B. Nygaard, Kristen M. Hitchcox, Kathleen R. Markan, K. N. & Michael F. Hirshman, Yu-Hua Tseng, and L. J. G. Brown adipose tissue regulates glucose homeostasis and insulin sensitivity. *J. Clin. Invest.* **123,** 215–223 (2013).

63. Bartelt, A. *et al.* Brown adipose tissue activity controls triglyceride clearance. *Nat. Med.* **17,** 200–206 (2011).

64. Wu, M. V., Bikopoulos, G., Hung, S. & Ceddia, R. B. Thermogenic capacity is antagonistically regulated in classical brown and white subcutaneous fat depots by high fat diet and endurance training in rats: Impact on whole-body energy expenditure. *J. Biol. Chem.* **289,** 34129–34140 (2014).

65. Ikeda, K. *et al.* UCP1-independent signaling involving SERCA2b- mediated calcium cycling regulates beige fat thermogenesis and systemic glucose homeostasis. *Nat. Publ. Gr.* **23,** (2017).

66. Ukropec, J., Anunciado, R. P., Ravussin, Y., Hulver, M. W. & Kozak, L. P. UCP1-

independent thermogenesis in white adipose tissue of cold-acclimated Ucp1-/-mice. *J. Biol. Chem.* **281,** 31894–31908 (2006).

67. Seoane-Collazo, P. *et al.* Hypothalamic-autonomic control of energy homeostasis. *Endocrine* **50,** 276–291 (2015).

68. Feldmann, H. M., Golozoubova, V., Cannon, B. & Nedergaard, J. UCP1 Ablation Induces Obesity and Abolishes Diet-Induced Thermogenesis in Mice Exempt from Thermal Stress by Living at Thermoneutrality. *Cell Metab.* **9,** 203–209 (2009).

69. So, M., Gaidhu, M. P., Maghdoori, B. & Ceddia, R. B. Analysis of time-dependent adaptations in whole- body energy balance in obesity induced by high- fat diet in rats. *Lipids Health Dis.* **10,** 99 (2011).

70. Shimizu, I. & Walsh, K. The Whitening of Brown Fat and Its Implications for Weight Management in Obesity. 224–229 (2015). doi:10.1007/s13679-015-0157-8

71. Shimizu, I. *et al.* Vascular rarefaction mediates whitening of brown fat in obesity. *J. Clin. Invest.* **124,** 2099–2112 (2014).

72. Peterson, C. M. *et al.* The thermogenic responses to overfeeding and cold are differentially regulated. *Obesity* **24,** 96–101 (2016).

73. Rothwell, N. J. & Stock, M. J. A role for brown adipose tissue in diet-induced thermogenesis. *Nature* **281,** 31–5 (1979).

74. Young, J. B., Saville, E., Rothwell, N. J., Stock, M. J. & Landsberg, L. Effect of diet and cold exposure on norepinephrine turnover in brown adipose tissue of the rat. *J. Clin. Invest.* **69,** 1061–71 (1982).

75. Gaidhu, M. P. *et al.* Chronic AMP-kinase activation with AICAR reduces adiposity by remodeling adipocyte metabolism and increasing leptin sensitivity. *J Lipid Res* **52,** 1702–1711 (2011).

76. Cannon, B. & Nedergaard, J. in *Adipose Tissue Protocols* (ed. Ailhaud, G.) 295–304 (Humana Press Inc., 2001).

77. Fine, J. B. & DiGirolamo, M. A simple method to predict cellular density in adipocyte metabolic incubations. *Int. J. Obes. Relat. Metab. Disord.* **21,** 764–8 (1997).

78. Gaidhu, M. P. *et al.* Prolonged AICAR-induced AMP-kinase activation promotes energy dissipation in white adipocytes : novel mechanisms integrating HSL and ATGL. *J Lipid Res* **50,** 704–715 (2009).

79. Dole, P. & Meinertz, H. Microdetermination of Long-chain Fatty Acids in Plasma and Tissues *. *J Biol Chem* **235,** 2595–2599 (1980).

80. Folch, J., Lees, M. & Sloane Stanley, G. H. A simple method for the isolation and purification of total lipides from animal tissues. *J. Biol. Chem.* **226,** 497–509 (1957).

81. Gaidhu, M. P., Fediuc, S. & Ceddia, R. B. 5-Aminoimidazole-4-carboxamide-1- ␣ - D - ribofuranoside- induced AMP-activated Protein Kinase Phosphorylation Inhibits Basal and Insulin-stimulated Glucose Uptake , Lipid Synthesis , and Fatty Acid Oxidation in

Isolated Rat Adipocytes *. *J Biol Chem* **281,** 25956–25964 (2006).

82. Livak, K. J. & Schmittgen, T. D. Analysis of Relative Gene Expression Data Using Real-Time Quantitative PCR and the 2−ΔΔCT Method. *Methods* **25,** 402–408 (2001).

83. Lapa, C. *et al.* Whitening and Impaired Glucose Utilization of Brown Adipose Tissue in a Rat Model of Type 2 Diabetes Mellitus. *Sci. Rep.* **7,** (2017).

84. Nye, C. K., Hanson, R. W. & Kalhan, S. C. Glyceroneogenesis Is the Dominant Pathway for Triglyceride Glycerol Synthesis in Vivo in the Rat *. **283,** 27565–27574 (2008).

85. Srivastava, S., Baxa, U., Niu, G., Chen, X. & Veech, R. A Ketogenic Diet Increases Brown Adipose Tissue Mitochondrial Proteins and UCP1 Levels in Mice. *IUBMB Life* **65,** 1–20 (2013).

Appendix

A. Adipocyte Isolation

1. Extract iBAT and aBAT and carefully trim away any muscle, connective tissue, and white fat. Combine iBAT and aBAT to maximize the yield of brown adipocytes.
2. Incubate the tissues in a 50 ml falcon tube containing Krebs-Ringer Buffer (0.154 M NaCl, 0.154 M KCl, 0.11 M CaCl2, 0.154 M MgSO4, 0.154 M KH2PO4, 0.154 M NaHCO3, pH 7.4) with 5.5 mM glucose, 30 mM HEPES (KRBH) and 4% BSA, supplemented with collagenase (0.83 mg/ml) at 37°C under orbital agitation (120 orbital strokes/ min) for 5 min.
3. Vortex the combined tissues for 5 seconds
4. Filter the tissues and discard the filtrate
5. Finely mince the remaining tissues with surgical scissors and incubate them in fresh KRBH-4% BSA containing collagenase (0.83 mg/ml) at 37°C under orbital agitation (120 orbital strokes/ min) for about 20-30 min
6. Strain the digested tissue using a nylon mesh and isolate cells
7. Transfer the isolated cells to a 50 ml falcon tube
8. Add 5 ml of KRB to dilute the concentration of the collagenase and reduce its activity
9. Centrifuge the cells at 1000 RPM for 30 sec to allow the adipocytes to float to the top of the media
10. Aspirate the media slowly, leaving only the adipocytes in the falcon tube

11. Wash the adipocytes with KRBH and allow the cells to float and settle at the top of the media by leaving the falcon tube in the tube rack for 10 min
12. Repeat the wash and aspiration twice more
13. Resuspend the cells in KRBH containing 3.5%-FA free BSA (KRBH-3.5% BSA)
14. Count the number of cells present in the falcon tube
    a. Determine lipocrit height by swirling the falcon tube and transferring a 300 µl aliquot into a centrifuge tube. Centrifuge these cells at 1000 RPM for 30 s and measure the lipocrit height using a ruler.
    b. Determine cell diameter by swirling the falcon tube, transferring a 20 µl aliquot of adipocytes onto a glass slide and measuring their diameters under a light microscope
    c. Determine the number of cells available in the falcon tube by using the equation for calculating the volume of a sphere, the volume of media in the falcon tube and the lipocrit height in the centrifuge tube
15. Allocate the appropriate number of cells into each scintillation vial for subsequent assays

B. Free Glycerol Determination as a Measure of Lipolysis using the Sigma Free Glycerol Determination Kit (Cat. # FG0100-1KT)

1. Thaw the frozen media samples to be analyzed for free glycerol
2. Reconstitute the free glycerol reagent in 40 ml of water in the amber bottle containing the reagent
3. Stopper the vial and mix by gentle inversion
4. Store the reconstituted reagent in the dark
5. Add 10 µl of water, Glycerol Standard and sample to each pre-labelled cuvette
6. Pipette 800µl of the reconstituted glycerol reagent into each cuvette
7. Mix the sample and reagent by gently vortexing the cuvette
8. Incubate the cuvettes at 37°C for 5 min
9. Measure the absorbance (A) of the standard and samples on a spectrophotometer at 540nm.
10. Calculate the concentration of free glycerol in each sample using the equation:

$$= \frac{(A_{SAMPLE}-A_{BLANK})}{(A_{STANDARD}-A_{BLANK})} \text{ x Concentration of Standard}$$

C. Glucose and Palmitate Oxidation

1. Isolate and pipette $5x10^5$ adipocytes into scintillation vials containing 1.5 ml of KRBH-3.5% BSA with 0.2 μCi/ml D-[U-^{14}C] glucose and 5.5 mM non-labeled D-glucose KRBH-3.5% BSA or KRBH-3.5% BSA containing [1-^{14}C] palmitic acid and 200 μM non-labelled palmitate.
    a. To examine the effect of lipolysis on glucose/palmitate oxidation, add 100 nM of isoproterenol (Iso)
    b. To examine the differences between coupled and uncoupled respiration in these adipocytes, add 100 μM of oligomycin (Oligo).
        i. Following the addition of Oligo, swirl the scintillation vial and incubate it at room temperature for 15 min prior to the incubation with/without Iso
2. Carefully place a cap-less Eppendorf containing a loosely folded piece of filter paper in the scintillation vial
3. Seal the vial with a rubber cap
4. Incubate the scintillation vials for 1 h at 37°C with gentle agitation (80 orbital strokes/min).
5. Following the 1 h incubation period, use a syringe to soak the filter paper in the centered well with 200 μl of phenethylamine:methanol (1:1, vol:vol). This filter paper will collect $^{14}CO_2$
6. Following this, acidify the media using 5 N H_2SO_4 to release $^{14}CO_2$ from the adipocytes and media

7. Incubate the vials at 37°C for 1 h with gentle agitation (80 orbital strokes/min) for the collection of $^{14}CO_2$
8. Remove the filter paper from the centered well and place it into a separate scintillation vial containing 5 ml of scintillation fluid
9. Count for radioactivity

D. Glucose Uptake Assay

1. Isolate and pipette approximately $4x10^5$ cells per plastic vial
2. Incubate these cells for 1 h at room temperature with gentle agitation (80 orbital strokes/min)
3. 20 min prior to the end of the incubation, add 100 nM of insulin to the insulin-treated tubes
4. Add KRBH-1% BSA containing 0.5 mM 2-deoxy-D-glucose and 0.5 μCi of 2-[1,2-^{3}H]deoxy-D-glucose to the cells for 3 min
5. Terminate the incubations by adding 10 μl of 1.5 mM cytochalasin B to the cells
6. Take 240 μl aliquots of the cell suspensions and transfer them into plastic microtubes already containing 125 μl of di-"isononyl" phthalate
7. Centrifuge the tubes for 30 sec (6000 x g) to separate the adipocytes from the radioactive incubation medium
8. Using a sharp scalpel or box-cutter, cut through the oil phase of the tube that now sits between the medium and the adipocyte suspension
9. Transfer the portion of the tube containing the adipocytes to a scintillation vial containing 5 ml of scintillation fluid
10. Count for radioactivity
11. Total count must be adjusted for non-specific transport. Measure non-specific transport by having two additional plastic tubes with the adipocyte suspension. Instead of adding the radioactive medium first, add cytochalasin B.
12. Subtract non-specific counts from all other counts

E. Glycerol Incorporation into Lipids

1. Isolate and pipette $5x10^5$ cells into scintillation vials containing 1.5 ml of KRBH-3.5% BSA containing 0.2 μCi/ml of [^{14}C(U)] glycerol
2. Seal the vials with rubber caps and incubate for 1 h at 37°C with gentle agitation (80 orbital strokes/min)
3. Remove the rubber caps and add 5 ml of Dole's Reagent
    a. Dole's Reagent: 40:10:1 (isopropanol:hepane: 0.5 M H_2SO_4)
4. Tightly seal the scintillation vial with a cap and vortex for 1 min
5. Uncap the scintillation vial and add 3 ml of ddH_2O and heptane, in sequence
6. Tightly seal the scintillation vial again and vortex for 1 min
7. Let the scintillation vial sit for a minimum of 20 min to allow the phases to separate
8. Extract 1 ml of the top heptane phase and place in a separate, pre-weighed scintillation vial
9. Allow the scintillation vial to dry overnight in a laminar fume hood
10. Weigh the dried scintillation vial the next day to obtain a lipid weight measurement
11. Add 5 ml of scintillation fluid and count for radioactivity

F. Lactate Determination using the Biovision Lactate Colorimetric/Fluorimetric Assay Kit (Cat. # K607-100)

1. Thaw the frozen media samples to be analyzed for lactate production
2. Rinse 10-kDa molecular weight spin filters in 2 ml Eppendorf tubes using ddH_2O
3. Add ddH_2O to spin filters and centrifuge at 13, 000 RPM for 5 min
4. Discard the ddH_2O from the filters and allow them to dry
5. Add 100 µl of the sample to the filter and spin at 13, 000 RPM for 5 min at 4°C
6. Following deproteination of the sample, remove the filter and extract the sample from the bottom of the Eppendorf.
7. Using the Lactate Assay Kit, mix 990 µl of the Lactate Assay Buffer with 10 µl of the Lactate Standard to produce the Assay Standard
8. Load 2, 4, 6, 8 and 10 µl of the Assay Standard into a 96-well plate and bring total volume to 50 µl with Lactate Assay buffer.
9. Load 2-50 µl of sample and bring total volume to 50µl with Lactate Assay Buffer
    - Note: In order to determine the optimal quantity of sample to load, a pilot run prior to the assay is recommended using varying volumes of sample
10. Add 46 µl of Lactate Assay Buffer, 2 µl of resuspended Lactate Enzyme and 2 µl of the Lactate Probe per well
11. Mix reaction mixes well and incubate the 96-well plate for 30 min in the dark
12. Read the plate at 570nm in a plate reader.

G. Palmitate Incorporation into Lipids

1. Palmitate Incorporation into Lipids

1. Isolate and pipette $5x10^5$ cells into scintillation vials containing 1.5 ml of KRBH-3.5% BSA containing 0.2 μCi/ml of [1-^{14}C] palmitate and 200 μM of non-labelled palmitate
2. Seal the vials with rubber caps, gasify for 15 seconds with carbogen gas and incubate for 1 h at 37°C with gentle agitation (80 orbital strokes/min)
3. Following the 1 h, transfer 2 ml of the adipocyte suspension and radioactive incubation medium into 2 ml Eppendorf tubes.
4. Centrifuge the samples at 3000 x g for 1 min
5. Discard the radioactive medium and wash the cells with 1 ml of PBS
6. Centrifuge the samples at 3000 x g for 1 min
7. Repeat steps 5-6 twice more
8. After the third wash, discard the PBS
9. Freeze the adipocytes at -80°C until lipid extraction

2. Lipid Extraction using Folch's Method[80]

1. Take samples out of the -80°C freezer
2. Resuspend cells in 600 μl of cholorform:methanol (2:1 vol:vol)
3. Vortex the cells for 30 s
4. Spin the samples at 3000 x g for 5 min at 4°C
5. Transfer 300 μl of the upper cholorform phase into a new Eppendorf tube
6. Allow the tubes to evaporate under nitrogen gas overnight
7. Resuspend in 50 μl of chloroform:methanol (2:1, vol:vol)

3. Thin Layer Chromatography (TLC)

1. On a Whatman TLC plate, using a pencil, draw a line 2 cm from the bottom of the plate
2. Load 4 µl of TAG standard (triolein) and 4 µl of sample along this line
3. Using a TLC unit, add 200 ml of your hexane:diethyl ether:acetic acid (70:30:1, vol:vol:vol) mobile phase to the bottom of the unit
4. Place the plate loaded with your samples into the TLC unit
5. Allow the mobile phase to run up ~80% of the plate
6. Remove the plate from the unit and allow both to air dry for 10 min
7. Place the plate back into the TLC unit and add iodine. The iodine vapours will allow for visualization of the spots corresponding to the TAG.
8. Once the spots are visible, remove the plate from the unit and scrape off the spots that are aligned with the TAG standard
9. Add the scraped residue into a scintillation vial containing 5 ml of scintillation fluid
10. Count for radioactivity

H. Measuring Gene Expression in BAT using PCR

1. RNA Extraction using TRIzol™

1. Sterilize work environment and consumables
2. Transfer 50 mg of tissue into 2 ml tube containing 1 ml of TRIzol
3. Using a mechanical homogenizer, homogenize the samples
4. Incubate the samples for 5 min at room temperature to allow for the dissociation of the nucleoproteins complex.
5. Add 200 µl of chloroform to each tube
6. Vortex each tube vigorously for 15 sec
7. Incubate the samples for 2-3 mins at room temperature
8. Centrifuge the samples at 13, 000 RPM for 15 mins at 4°C

2. RNA Isolation

1. Extract the aqueous (top) phase and avoid the other two phases.
2. Move the aqueous phase into a new, sterile, 1.5 ml Eppendorf tube
3. Add 500 µl of 100% isopropanol to the aqueous phase and mix by inverting the tube several times
4. Incubate the samples at room temperature for 10 min
5. Centrifuge the samples at 13, 000 RPM for 20 min at 4°C.
6. Following centrifugation, a pellet should be visible at the bottom of the tube
7. Discard the supranatant and wash the pellet with 1 ml of 75% ethanol.
8. Centrifuge the tubes 13, 000 RPM for 20 min at 4°C.
9. Repeat steps 14-16 to perform a second wash of the pellet
10. Discard the supranatant.

11. Air dry the pellet for 5-10 min

3. RNA Resuspension

1. Resuspend the pellet in 20 µl of sterile ddH_2O by pipetting in and out several times
2. Assess the concentration and quality of the RNA sample by Nanodrop
3. Proceed to cDNA synthesis or store samples at -80°C until use

4. cDNA Synthesis using ABM EasyScript™ Reverse Transcriptase cDNA Synthesis kit

1. Thaw RNA samples and reagents on ice
2. Add 2 µg of each RNA sample to sterile tubes
3. Bring total volume to 12.5 µl with ddH_2O
4. Add 1 µl of random primers and 1 µl of dNTP mix to each sample
5. Centrifuge briefly
6. Incubate samples at 65°C for 5 min
7. Incubate samples on ice for one min
8. Centrifuge briefly
9. Make a master mix containing 4 µl of 5X RT buffer, 0.5 µl of RNAse OFF Ribonuclease Inhibitor and 1 µl of OneScript mix, per sample
10. Add 5.5 µl into each tube
11. Mix components well and collect with centrifuge
12. Incubate samples at 25°C for 10 min
13. Perform cDNA synthesis by incubating the tube for 50 min at 42°C
14. Stop the reaction by heating the samples at 85°C for 5 min

15. Incubate on ice.
16. Proceed to PCR or store cDNA samples at -20°C.

5. PCR

1. Thaw cDNA samples
2. In a 96-well plate, load 10 ng of cDNA per well.
3. To each sample, add 0.4 µl of the primer of interest, 5.6 µl of ddH_2O and 10 µl of Brightgreen 2x qPCR Mastermix
4. Centrifuge the plate at 2000 RPM for 5 min at 4°C
5. Perform qPCR analysis by using the following amplification conditions:
    - 95°C (10 min); 40 cycles of 95°C (15 s), 65°C (1 min); a 0.5°C step-wise increment from 65°C to 95°C.
6. Normalize the results to the control gene β-acting and calculate fold change using the ΔΔCt method[82].

I. Western Blotting: Protein Extraction

1. Following extraction, tissue is immediately frozen in liquid nitrogen and stored at -80°C until homogenization
2. Move 50 mg of BAT into 2 ml Eppendorf tubes already containing 200 µl of lysis buffer (25 mM Tris-HCl, 25 mM NaCl (pH 7.4), 1 mM $MgCl_2$, 2.7 mM KCl, 1% Triton-X and protease and phosphatase inhibitors)
3. Using a mechanical homogenizer, homogenize the tissue sample
4. Sonicate sample 3X for 3 seconds each time at 40% amplitude
5. Following this, centrifuge the samples at 13, 000 RPM at 4°C for 10 min
6. Remove the samples from the centrifuge and extract the protein lysate from the Eppendorf, avoiding the pellet that formed at the bottom of the tube
7. Transfer the lysate into a separate, clean Eppendorf
8. Extract an aliquot for protein quantification using the Bradford method.
9. Samples can be used immediately for Western Blotting or can be stored at -80°C and used at a later date.

1. Lysate Preparation with Laemli

1. Prepare 50µl of 2-mercaptoethanol in 950µl of 2X Lameli buffer.
2. Dilute samples 1:1 with Laemli buffer
3. Boil lysate/laemli at 95°C for 5 mins
4. Centrifuge lysate/laemli briefly
5. Proceed to Western blot

J. Western Blotting

1. Western Blot Gel Components

1.1. 1.5 M Tris-HCl, pH 8.8

27.3 g of tris Base

80 ml of deionized water

Adjust to pH 8.8 with 6N HCl

Bring total volume to 150 ml with deiodinized water

1.2. 0.5 M Tris-HCl

6 g of Tris base

60 ml of deiodinized water

Adjust to pH 6.8 with 6N HCl

Bring total volume to 100 ml with ddH_2O water

1.3. 10X Electrode (Running) buffer, pH 8.3 (1 L)

30.3 g of Tris base

144 g of Glycine

10 g of SDS

Dissolve and bring the total volume to 1L with ddH_2O

1.4. 10% APS

Dissolve 100 mg of ammonium persulfate in 1 ml of ddH2O.

Make APS fresh each time

2. Western Blot Gel Formulations

2.1. Resolving Gel

1. Prepare the monomer solution by mixing appropriate quantities of the following reagents:

% Gel	ddH2O (ml)		30% Acrylamide/Bis (ml)		Gel buffer (ml) 1.5M Tris-HCl, pH 8.8		10% (w/v) SDS (ml)	
	2 Gels	4 Gels	2 Gels	4 Gels	2 Gels	4 Gels	2 Gels	4 Gels
7%	7%	8.61	17.23	3.97	7.93	4.25	8.5	0.17
8%	8.05	16.1	4.53	9.06	4.25	8.5	0.17	0.34
10%	6.91	13.82	5.67	11.34	4.25	8.5	0.17	0.34
12%	5.78	11.56	6.8	13.6	4.25	8.5	0.17	0.34

2. APS and TEMED are added last. For one gel, add 100 µl of 10% APS and 10 µl of TEMED. Mix well and add the gel preparation into the plate

2.2. Stacking Gel (4% Gel)

ddH2O (ml)		30% Acrylamide/Bis (ml)		Gel buffer (ml) pH 6.8		10% (w/v) SDS (ml)	
2 Gels	4 Gels	2 Gels	4 Gels	2 Gels	4 Gels	2 Gels	4 Gels
3.94	7.88	0.87	1.73	1.63	3.25	0.065	0.13

3. Similar to the preparation for the resolving gel, only add 10% APS and TEMED following the mixture of the other components
4. For 1 gel add 50 µl of 10% APS and 5 µl of TEMED
5. Mix well and add to the top of the Resolving Gel in the plates
6. After filling the plates with the stacking gel, gently insert the well combs
7. Allow the gels to polymerize for 15-20 minutes

3. Loading the Gel

1. Once the gels have polymerized, place the plates into running clamps and insert the clamps into a running apparatus
2. Fill the running apparatus with 1X Running Buffer
3. Gently remove the well combs
4. Load 25 μg of protein into each well
5. Once all wells are loaded, run the gel at 110V for 2 h

4. Transfer

4.1. Transfer Buffers

4.1.1. 10X Transfer Buffer

25 mM Tris base

192 mM Glycine

Dissolve in make total volume to 1 L of ddH_2O

4.1.2. 1X Transfer Buffer (1 L)

700 ml of ddH2O

200 ml of methanol

100 ml of 10X transfer buffer

5.2. PVDF Membrane Activation

1. Place pre-cut PVDF membranes into a container
2. Submerge the membranes with 100% methanol
3. Leave membranes in methanol for 30 s
4. Discard the methanol and quickly rinse the membranes with ddH_2O before submerging them for 2 min in ddH_2O

5. Discard the ddH_2O and pour 1X Transfer Buffer over the membranes
6. Allow membranes to equilibrate for 10 minutes

5.3. Wet Transfer Protocol

1. Prepare a casserole dish with transfer cassettes, fiber pads and pre-cut filter paper
2. Add enough 1X Transfer buffer to the casserole dish to cover the bottom and to soak the filter paper and fiber pads
3. Assemble the bottom of the cassette by adding a fiber pad, followed by 2, pre-soaked filter papers
4. Remove one set of plates containing a gel from the running apparatus
5. Carefully separate the two plates using a flat pick and transfer the gel onto the filter paper in the transfer cassette
6. Once the gel is centered on the filter paper, carefully place a membrane on top of the gel
7. Roll the top of the membrane to remove any bubbles from in between the membrane and the gel
8. Place a filter paper on top of the membrane and roll it again
9. Place a second filter paper on top of the previous one and roll it a final time
10. Add a pre-soaked fiber pad to the top of the second filter paper and clamp the cassette shut.
11. Place the casette in the transfer apparatus
12. Close the transfer apparatus and incubate it at 4°C
13. Set the transfer to 120V for 2 h

5. Probing the Membrane

5.1. Buffers

5.1.1. 10X Wash Buffer (1 L)

60.57 g of Tris base

87.66 g of NaCl

5.1.2. 1X Wash Buffer (1 L)

Dilute to 1X using ddH_2O

Add 500 µl of Tween

Add 500 µl of NP40

5.1.3. Blocking Buffer (3% BSA)

Dissolve 1.5 g of crude BSA in 50 ml of 1X Wash buffer

5.2. Blocking the Membrane

1. After the transfer is complete, prepare containers with 8 ml of blocking buffer in each
2. Remove the membrane from the transfer apparatus and place it in one of the containers immediately
3. Shake for 1 h

5.3. Incubation with Primary Antibody

4. Dilute the antibody of interest in blocking buffer
    - Note: dilutions vary based on the affinity of the antibody for the protein and the abundance of the protein in the lysate
5. Discard the blocking buffer that was shaking over the membrane and immediately add the primary antibody preparation

6. Incubate the membrane in this antibody for 2 h at room temperature with gentle shaking
7. After two hours, discard the primary antibody dilution
8. Wash the membrane with 1X wash buffer 5x10 min

5.4. Incubation with Secondary Antibody

9. Dilute the secondary antibody in blocking buffer
10. Discard the wash buffer
11. Immediately add the secondary antibody
12. Incubate for 1 h at room temperature with gentle shaking
13. After 1 h, wash the membrane with 1X wash buffer 5x10 min

5.5. Developing the Membrane

14. Discard the secondary antibody and allow any excess liquid to run out of the containers
15. Add Luminata Western HRP Chemiluminescent Substrate (Luminata) to the membranes and shake gently by hand for 2 min
16. Discard the Luminata
17. Remove the membranes from the containers and place them in film development cassettes
18. In a dark room, expose film to the membranes for varying amounts of times to obtain different exposures
19. After the desired exposure time passes, remove the film from the development cassettes
20. Dip the film in Developer Fluid until bands begin to appear

21. After the bands become visible, immediately wash the film in water and fix in Fixer Fluid until film loses opaque blotches.
22. When film is completely transparent, wash off residual Fixer Fluid with water